J. Fluid Mech. (2011), *vol.* 687, *pp.* 1–40.
doi:10.1017/jfm.2011.294

Particle dynamics in the channel flow of a turbulent particle–gas suspension at high Stokes number. Part 1. DNS and fluctuating force model

Partha S. Goswami and V. Kumaran†

Department of Chemical Engineering, Indian Institute of Science, Bangalore 560 012, India

(Received 2 July 2010; revised 24 June 2011; accepted 4 July 2011;
first published online 6 October 2011)

The fluctuating force model is developed and applied to the turbulent flow of a gas–particle suspension in a channel in the limit of high Stokes number, where the particle relaxation time is large compared to the fluid correlation time, and low particle Reynolds number where the Stokes drag law can be used to describe the interaction between the particles and fluid. In contrast to the Couette flow, the fluid velocity variances in the different directions in the channel are highly non-homogeneous, and they exhibit significant variation across the channel. First, we analyse the fluctuating particle velocity and acceleration distributions at different locations across the channel. The distributions are found to be non-Gaussian near the centre of the channel, and they exhibit significant skewness and flatness. However, acceleration distributions are closer to Gaussian at locations away from the channel centre, especially in regions where the variances of the fluid velocity fluctuations are at a maximum. The time correlations for the fluid velocity fluctuations and particle acceleration fluctuations are evaluated, and it is found that the time correlation of the particle acceleration fluctuations is close to the time correlations of the fluid velocity in a 'moving Eulerian' reference, moving with the mean fluid velocity. The variances of the fluctuating force distributions in the Langevin simulations are determined from the time correlations of the fluid velocity fluctuations and the results are compared with direct numerical simulations. Quantitative agreement between the two simulations are obtained provided the particle viscous relaxation time is at least five times larger than the fluid integral time.

Key words: particle/fluid flow, turbulent flows

1. Introduction

Particle-laden turbulent flows find applications in many industrial processes such as energy conversion, air pollution control, etc. In these types of flows, there is a strong coupling between the turbulent fluctuations in the fluid velocity fields, and the fluctuating velocities of the particles. There have been several experimental and simulation studies of the effect of particle fluctuations on the fluid turbulence. A compilation of experimental data by Gore & Crowe (1989) indicated that small particles with size an order of magnitude smaller than the integral length scale of the fluid will attenuate the turbulence, while large particles will increase the intensity.

† Email address for correspondence: kumaran@chemeng.iisc.ernet.in

Kulick, Fessler & Eaton (1994) did the experiments on vertical channels using particle Stokes numbers (St) ranging from 0.57 to 3.0 with a mass loading up to 80 %, to investigate the turbulence attenuation. Fessler, Kulick & Eaton (1994) investigated the instantaneous particle concentration at the centre-plane of a vertical turbulent channel flow. Khalitov & Longmire (2003) reported the results of their channel flow experiments, mainly focusing on the two point gas–particle and particle–particle correlation for Stokes number (based on the integral time scale) in the range 0.2 to 10, and observed that the gas–particle covariance becomes very small when the Stokes number is $\geqslant 5$. Recently Gerashchenko *et al.* (2008) have investigated two-dimensional Lagrangian acceleration statistics of inertial particles in a turbulent boundary layer adjacent to a plate, and found that as the plate is approached, the tails of the probability density functions become narrower, and their peak occurs at negative accelerations. Tanaka & Eaton (2008) introduced the particle momentum number (Pa) to understand the phenomenon of turbulence modification by particles in the particle-laden flows. One of the earliest numerical simulations of particle-laden turbulent flows was performed by Riley & Patterson (1974) to study the particle dispersion in decaying isotropic turbulence. Squires & Eaton (1991) investigated the effect of isotropic turbulence on the concentration field of the heavy particle. Elghobashi & Truesdell (1992) used direct numerical simulation (DNS) to investigate particle dispersion in decaying isotropic turbulence when the particles' relaxation time is of the order of the Kolmogorov time scale, and presented the results of time development of the mean square displacement of the particles, Lagrangian autocorrelation and the turbulent diffusivity of the particle and the fluid points. Squires & Eaton (1990) and Elghobashi & Truesdell (1993) studied the effect of particle fluctuations on homogeneous turbulence. Bec *et al.* (2006) used DNS to study the particle acceleration distribution in the case of isotropic turbulence for a range of particle Stokes numbers from $St_K = 0.16$ to 3.5. They defined the Stokes number as the ratio of particle relaxation time to the Kolmogorov time scale. Bec *et al.* (2010) have investigated the intermittent relative velocity statistics of the inertial particle in isotropic turbulent suspension. Such studies are important in developing the model for collision kernels. The study of Bec *et al.* (2010) shows that as $St_K > 10$, particles move ballistically in the flow with uncorrelated velocities, and the structure functions become independent of the separation distance of the particles. In our simulations, the Stokes number St_K based on the Kolmogorov scale is $\sim$24 times larger than the Stokes number based on the integral time scale discussed in the next section. We are working in the regime where the Stokes number based on the Kolmogorov scale is much larger than 10 in most cases, and so the particle velocities can be considered uncorrelated.

Li & McLaughlin (2001) reported the effect of particle feedback on turbulence, and the particle concentration profile in the case of a vertical channel flow for particle of relaxation time $(\tau_v) \sim 200$ when scaled by the wall unit. They have reported the variation of particle concentration and the particle mean square velocity-fluctuations along the cross-stream direction. Rouson & Eaton (2001) investigated the preferential particle concentration field in the case of passive transport of particles by fully developed channel flow, for particles with time constant 0.6–56 based on the centreline Kolmogorov time scale, and found that preferential concentration occurs for Stokes numbers of the order of unity. Yamamoto *et al.* (2001) have performed large eddy simulation (LES) including inter-particle collision. They have done the simulation for Stokes numbers up to 70 based on the inverse of the shear rate (which turns out to be $\sim$200 based on the wall time unit). Carlier, Khaliji & Osterle (2005) have investigated the dispersion of small particles in turbulent shear flow by modelling the

directional dependency of fluid Lagrangian time scales. Fevrier, Simonin & Squires (2005) have investigated the velocity distribution of the heavy particles in the dilute gas–solid turbulent flow. They have introduced the concept of partitioning of the particle velocities into mesoscopic Eulerian particle velocity fields. Kraichnan (1958) analysed the hydromagnetic turbulence using a homogeneous force with a Gaussian distribution for the fluid phase. Fouxon & Horvai (2008) have introduced the Langevin description for the separation dynamics of the particles when the particle relaxation time is comparable to the inertial time scale of the turbulent flow. Later Lavezzo *et al.* (2010) performed DNS of turbulent channel flow with suspended inertial particles to investigate the effect of shear and gravity on the particle acceleration distribution. Recently, Balachandar & Eaton (2010) have reviewed the experimental and computational techniques for turbulent dispersed multiphase flows, their strengths and limitations.

Goswami & Kumaran (2010*a*) investigated the effect of fluid velocity fluctuations on the statistics of the particle velocity and accelerations in a turbulent gas–solid suspension for Couette flow where the particle relaxation time is large compared to the correlation time for the fluid velocity fluctuations. It was found that the distribution of particle velocities is very different from Gaussian, especially in the spanwise and wall-normal directions. However, the distribution of the acceleration fluctuation of the particles is found to be close to Gaussian, though the distribution is highly anisotropic. The distribution of the acceleration fluctuations of the particles are very well approximated by the distribution evaluated from the fluid velocity fluctuations when there is one-way coupling (effect of fluid on particles is included), indicating that there is no correlation between the particle and fluid velocities in this case. Goswami & Kumaran (2010*b*) have developed a fluctuating force model for representing the effect of the turbulent fluid velocity fluctuations on the particle phase in a shear-driven turbulent gas–solid suspension in the limit of high Stokes number, when the particle relaxation time is large compared to the fluid time scale, and found that the fluctuating force simulation is able to quantitatively predict the concentration and mean velocity profiles, the mean square velocities and also the distribution of the fluctuating velocities for the two distinct regimes: where the viscous relaxation time is small compared to the time between collisions, as well at higher volume fractions where the time between collisions is small compared to the viscous relaxation time of the particle.

In the present analysis, we investigate the effect of turbulence on the particle velocity fluctuations as a function of the ratio of the viscous relaxation time for the particles and the time between collisions in a vertical channel. In contrast to Couette flow, the fluid velocity variances in the different directions in a channel are highly non-homogeneous, and they exhibit significant variation across the channel. Throughout the analysis, the particle size is considered to be small enough that the Reynolds number based on the relative instantaneous velocity of the particle, the gas density and viscosity, $Re_p = \rho_f d v_r / \eta$, is in the range $Re_p = 0.8$ to 10. The Stokes number, which is the ratio of particle relaxation time and fluid integral time scale, $St = (\tau_v / \tau_f)$, is large (2.5–30). If the drag force is given by Stokes' law, the viscous relaxation time is given by $\tau_v = \rho_p d^2 / 18\eta$. It is also useful to define the Stokes number St_K based on the Kolmogorov time scale for the turbulent flow. The Kolmogorov time scale increases by a factor of $\sim$6 from the near-wall region to the channel centre. The Stokes number based on the minimum Kolmogorov time scale is around 24 times higher than the Stokes number based on the fluid integral time scale, that is, $St_K = 24 \times St$. Here, the Kolmogorov time scale is defined as $\tau_\eta = (\nu / \epsilon)^{1/2}$,

Simulation run	ρ_p	ϕ_s	$2\delta/d_p$	τ_v	$\tau_{c_{pp}}$	$\tau_{c_{pw}}$	St
(*a*) $\tau_v < \tau_{c_{pp}}$							
1	1000			177.7	1400.0	925.9	2.9
2	2000			355.3	1650.3	990.1	5.8
3	3000	9.44×10^{-5}	119.0	533.0	1807.7	978.4	8.6
4	4000			710.6	1999.0	1016.4	11.5
(*b*) $\tau_{c_{pp}} < \tau_v$							
5	1000			675.6	617.4	777.6	10.9
6	1500			1013.3	708.7	818.6	16.4
7	2000	7.0×10^{-4}	61.0	1351.1	774.3	846.2	21.9
8	3000			2026.6	912.0	939.6	32.8

TABLE 1. Particle–particle and particle–wall collision time ($\tau_{c_{pp}}$ and $\tau_{c_{pw}}$, respectively) for particles with different relaxation times (τ_v) and for different solid volume fractions (ϕ_s), scaled by (ν/u_*^2). The Reynolds number based on the channel half-width and centreline air velocity is $Re = 1994.7$, and that based on the channel half-width and friction velocity is 115.5. In all simulations, the particle diameter is assumed to be 39 μm (to be compared with experiments in Goswami & Kumaran 2011) and the number of particles in the simulation cell is 8000. The ratio of the particle diameter to the smallest Kolmogorov scale (d_p/η_K) varies between 0.4 (for $\tau_v < \tau_{c_{pp}}$) and 0.7 (for $\tau_{c_{pp}} < \tau_v$). ρ_p, particle density.

where ν is the kinematic viscosity and ϵ is the local rate of dissipation of turbulent kinetic energy. The minimum Kolmogorov time in wall units is 2.6.

The fluid and particle velocity fluctuations in the channel are analysed using two procedures. The first is direct numerical simulation (DNS) of the fluid equations in order to determine the fluid velocity fluctuations, and the forcing that these fluctuations cause in the particles. We use only one-way coupling, and neglect the effect of the forces exerted by the particles on the fluid turbulence. The direct numerical simulations are supplemented by fluctuating force simulations, using the Langevin model, where the fluid velocity fluctuations are substituted by random white noise in the equation for the particle motion. A Gaussian anisotropic random noise is used, and the second moments of the noise fluctuations are calculated from the turbulent fluid velocity fluctuations in the moving Eulerian reference frame, which moves with the local fluid velocities. The time decay of the fluctuations in the moving Eulerian reference frame is calculated from the DNS. An important assumption that the force is uncorrelated in time (white noise), which is valid only if the correlation time for the fluid velocity correlations is small compared to the viscous relaxation time of a particle.

Table 1 shows the parameter values for which we have carried out direct numerical simulations. In all cases, the fluid phase Reynolds number (Re) based on half of the channel width and the centreline gas velocity has been set equal to 1994.7. The total number of particles in the simulation cell was fixed at 8000, because of computational limitations when the number of particles is too large. This imposes a limitation on the ratio of the channel width to particle diameter at fixed volume fraction, as shown in table 1. We have assumed that the particle diameter is 39 μm for calculating the viscous relaxation time in order to make a connection to real flows. This imposes a limitation on the channel thickness to ∼4 mm when the ratio of channel width and particle diameter is 100. This is smaller than the channel thickness of 1–10 cm

typically encountered in applications. However, increasing the number of particles by a factor of 10–100 would make it infeasible to probe the large range of parameters we have been able to access, as shown in table 1. The advantage of restricting the particle numbers is that we have been able to obtain profiles for all the particle concentration, velocity and fluctuating velocity across the entire channel over a range of parameters. The viscous relaxation time was varied independently by changing the mass density of the particles. The average time between collisions was obtained by counting the total number of collisions in the simulation, and dividing by the period of the simulation. Since the channel width is small, particles sometimes travel from one wall to the other without colliding with other particles. Therefore, we have also independently calculated the average time between particle–particle collisions and particle–wall collisions. The Stokes number in the present case is also reported as the ratio of the integral time scale to the particle viscous relaxation time. Since, in the case of channel flow, the integral time scale varies in the wall-normal direction, we have considered the maximum value of the fluid integral time scale for calculating the Stokes number. All length and velocity scales are reported in dimensionless form, and they are non-dimensionalized by the friction length and the friction velocity.

In § 2 we describe the governing equations for fluid and particle phases. Particle velocity and acceleration distributions, obtained from direct numerical simulation, are described in § 3. Section 4 describes the procedure and results for fluctuating force simulation with the analysis of different components of particle velocity fluctuations. Conclusions are given in § 5.

2. Governing equations for direct numerical simulation

The fluid phase is considered to be the incompressible Newtonian fluid which satisfies the Navier–Stokes equation for mass and momentum,

$$\boldsymbol{\nabla}\cdot\boldsymbol{u}=0, \tag{2.1}$$

$$\frac{\partial \boldsymbol{u}}{\partial t}+\boldsymbol{u}\cdot\boldsymbol{\nabla}\boldsymbol{u}=-\frac{1}{\rho_f}\boldsymbol{\nabla}p-\frac{1}{\rho_f}\frac{\mathrm{d}P}{\mathrm{d}x}e_x+\nu\,\boldsymbol{\nabla}^2\boldsymbol{u}, \tag{2.2}$$

where $\boldsymbol{u}(\boldsymbol{x},t)$ represents a three-dimensional instantaneous velocity field, ρ_f is the density of the fluid, $p(\boldsymbol{x},t)$ is the fluctuating pressure field, P is the external pressure field and ν is the kinematic viscosity. The velocity field satisfies the no-slip boundary conditions at the solid walls. Periodic boundary conditions in the streamwise (x) and spanwise (z) directions are used, as shown in figure 1, in order to obtain a fully developed two-dimensional flow with no variations in the mean fluid and particle properties in the streamwise and spanwise directions.

In the fluid flow equation we have not included the force exerted by the particles, therefore we only have one-way coupling of the fluid velocity fluctuations on the particle motion, as in the case of direct computation of shear-driven suspension by Goswami & Kumaran (2010*a*). The solid volume loading is $O(10^{-4})$, so we can neglect the particle volume effect. However, the mass loading is $(O\sim 1)$, and the turbulence field may be modified by the presence of the particles (Li & McLaughlin 2001). We have neglected this effect to focus our attention on the systematic study of the effect of turbulent flow fields on particle phase statistics using particles with different mass densities, and compared the results with those obtained from stochastic simulations based on the anisotropic and inhomogeneous turbulent diffusivity.

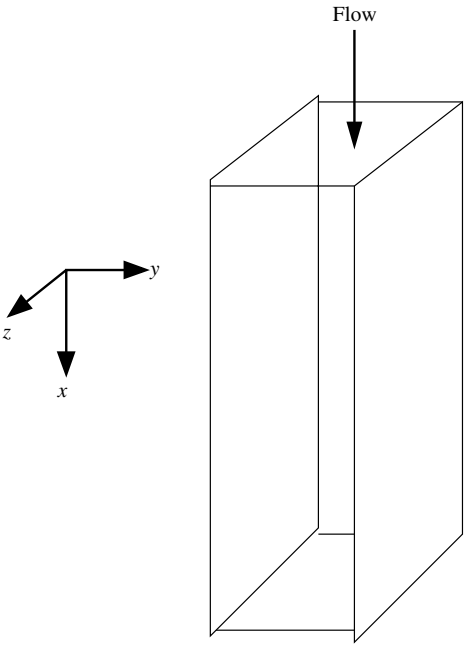

FIGURE 1. The flow geometry.

The equations of motion for the particle are

$$\frac{\mathrm{d}\boldsymbol{v}_i}{\mathrm{d}t} = \frac{\boldsymbol{u}_i(\boldsymbol{x}_{Pi}) - \boldsymbol{v}_i}{\tau_v} + \frac{1}{m_p}\sum_{i\neq j}\boldsymbol{F}_{ij} + \boldsymbol{g} \tag{2.3}$$

and

$$\frac{\mathrm{d}\boldsymbol{x}_i}{\mathrm{d}t} = \boldsymbol{v}_i, \tag{2.4}$$

where $\boldsymbol{u}_i(\boldsymbol{x}_{Pi})$ is the interpolated fluid velocity at the particle centre, $\boldsymbol{F}_{ij}$ is the force due to the instantaneous collision and $\boldsymbol{g}$ is the gravitational acceleration. When the particle Reynolds number is less than 1, the particle relaxation time is defined as

$$\tau_v = \frac{\rho_p d_p^2}{18\eta}, \tag{2.5}$$

where d_p is the particle diameter. If the particle Reynolds number is larger than 1, the corrected expression for τ_v is (Kumaran 2003)

$$\tau_v = \frac{\rho_p d_p^2}{18\eta\,(1+0.15\,Re_p^{2/3})}. \tag{2.6}$$

We have used the low-Reynolds-number limit of the expression of τ_v to make it easier for theoretical comparison, though there is substantial slip in the near-wall region and the Reynolds number is close to $O(10)$. Modifications to the drag law at higher particle Reynolds numbers can be included in both direct numerical simulation (DNS) and fluctuating force simulation (FFS) in a straightforward manner. Gravity acts on the particles in the direction of the mean flow.

Equation (2.3) is obtained by simplifying the original particle equation of motion described by Maxey & Riley (1983). The simplified equation of motion is obtained by neglecting the Saffman lift term, inertia of the virtual mass, Basset history term and considering $\rho_p \gg \rho_f$. The reason for the simplification has been described in detail by Goswami & Kumaran (2010*a*), and the relative magnitude of the forces has been quantified by Armenio & Fiorotto (2001). Goswami & Kumaran (2010*a*) discussed in detail the contribution of different authors to analysing the accuracy and the computational cost of different interpolation schemes. In the present computation we have used the same interpolation scheme used by Goswami & Kumaran (2010*a*). The algorithm for collision detection for the particle–particle and particle–wall collisions is the same as that used by Goswami & Kumaran (2010*a*).

In the coordinate system used here, the x, y and z axes are in the streamwise, wall-normal and spanwise directions, respectively. The origin of the coordinate system is located on one of the walls, as shown in figure 1. We have used the primitive variable formulation and coupled method to solve the Navier–Stokes equation using Kleiser–Schumann algorithm (Canuto, Hussaini & Zang 1988; Kleiser & Schumann 1980). The code for the two-phase channel flow was developed based on the open-source single-phase incompressible Navier–Stokes solver channel flow (Gibson 2007). We start the simulation by putting the particles randomly in the simulation box. The initial velocities are the interpolated fluid velocities at the particle position. Initially, we run the DNS for the air phase, and when it reaches the statistically stationary state (after time approximately 7000 in wall units), we initiate the particle dynamics. The duration of the initialization procedure for reaching steady state is $\sim$3–5 times the particle viscous relaxation time. After this, we start the sampling for a duration of 3–4 times the particle relaxation time.

We have non-dimensionalized the variables based on the wall units. The units of length and time are ν/u_* and ν/u_*^2, where ν and u_* are the kinematic viscosity and the friction velocity of the particle-free carrier phase. The friction velocity is defined as $u_* = (\tau_w/\rho)^{1/2}$, where τ_w is the wall shear stress. The size of our computational domain is $8\pi\delta \times 2\delta \times (4/3)\pi\delta$, where δ is the channel half-width. The domain is discretized into $128 \times 65 \times 64$ grids in the x, y and z directions, with a wall-normal stretching to capture the near-wall physics of the flow. The resolution in wall units (that is, scaled by (ν/u_*)) is 22.68 in the streamwise direction, 7.56 in the spanwise direction. In the wall-normal direction, it varies between 0.13 (near the wall) and 5.67 (at the centre). For all the simulations, the carrier phase is air at ambient conditions, and the simulation is done in isothermal conditions for which the kinematic viscosity is 1.4843×10^{-5} m^2 s^{-1}. The fluid phase Reynolds number based on the centreline velocity and half-width of the channel is 1997.4, while that based on the friction velocity, $Re_\tau = u_*\delta/\nu$, is 115.5. The channel centreline velocity scaled by the friction velocity is 17.2. If we use $d_p = 39$ μm, with particle density 1000 kg m^{-3}, and air viscosity at standard temperature and pressure, the viscous relaxation time is $\tau_v = 0.004\,8286$ s. The unit of time based on the kinematic viscosity and friction velocity (wall units) is $\nu/u_*^2 = 2.717\,9105$ s. In calculating the particle Stokes number (St), the maximum value of the fluid integral time scale is used, which is 61.7 in wall units. In the results section, all the variables are described in wall units unless explicitly mentioned. The different mass densities of the particles are varied by a factor of 4 in the simulations, as shown in table 1. The validation of the code is shown in figure 2.

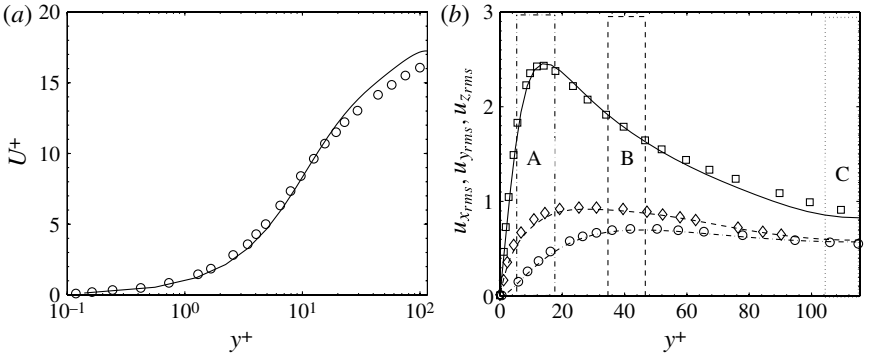

FIGURE 2. Air mean velocity (*a*) and root mean square velocity fluctuation (*b*). In (*a*), (—) is obtained from our simulation at $Re_\tau = 115.5$, and (○) is from Li & McLaughlin (2001) at $Re_\tau = 125$. In (*b*), $u_{x_{rms}}$ (—), $u_{y_{rms}}$ (-·-) and $u_{z_{rms}}$ (–) are obtained from present DNS and $u_{x_{rms}}$ (□), $u_{y_{rms}}$ (○) and $u_{z_{rms}}$ (◇) are obtained from Li & McLaughlin (2001). Different regions considered for distribution function calculations are A ($y^+ = 5.8$–17.3), B ($y^+ = 34.7$–46.2), and C ($y^+ = 104.0$–115.5).

3. Particle velocity and acceleration distributions from DNS

With the assumption that the force on the particle is given by the Stokes drag law, the particle acceleration $\boldsymbol{a}$ between collisions can be written as

$$\boldsymbol{a} = \frac{\boldsymbol{u} - \boldsymbol{v}}{\tau_v}, \tag{3.1}$$

where $\boldsymbol{u}$ is the instantaneous velocity of the fluid at the particle location, and $\boldsymbol{v}$ is the instantaneous particle velocity. The particle acceleration can be divided into a mean and a fluctuating component. The fluctuating part of the particle acceleration is

$$\boldsymbol{a}' = \boldsymbol{a} - \bar{\boldsymbol{a}} = \frac{\boldsymbol{u}' - \boldsymbol{v}'}{\tau_v}, \tag{3.2}$$

where $\boldsymbol{u}' = \boldsymbol{u} - \bar{\boldsymbol{u}}$ is the fluctuating fluid velocity at the particle location, and $\boldsymbol{v}' = \boldsymbol{v} - \bar{\boldsymbol{v}}$ is the fluctuating particle velocity at the particle location; $\bar{\boldsymbol{v}}$ is the average particle velocity at the particle location, and $\bar{\boldsymbol{u}}$ is the mean velocity of the fluid at the particle location. In calculating the velocity distribution function, we have considered the particle fluctuating velocity obtained by subtracting the local particle-averaged velocity from the instantaneous particle velocity. To obtain the particle-averaged velocity, the channel was divided into 50 intervals in the wall-normal direction, and the particle-averaged velocity was obtained by averaging over all the particles existing within each interval. There was no binning in the streamwise and spanwise directions, as both these directions are homogeneous and periodic. At any instant, there are more than 150 particles in each interval. After this, the distribution function is obtained by averaging over 20 000 'snapshots' of the flow. Following this procedure, the statistical standard deviation in the distribution function turns out to be approximately 5–6 % of the mean value (Goswami & Kumaran 2010*a*). Similarly, the average acceleration, which is proportional to the difference between the mean fluid and mean particle velocities, was subtracted while calculating the acceleration distribution function. It should be noted that while calculating the acceleration distribution, we have only included the local acceleration of the particles due to the effect of the fluid velocity, and we have neglected the acceleration during a collision. This is because the collision

processes are already included in the collision integral in theories for granular flows, and so they should not be incorporated into the random forcing due to turbulent fluctuations.

Since the mean and fluctuating velocity distributions in a channel are highly anisotropic, we analyse the probability distributions of the fluctuating velocities and accelerations over regions of thickness about ten wall units in the gradient directions at three locations, as shown in figure 2(*b*). The location A is located close to the wall of the channel where the gradient in the mean velocity is large, and the amplitude of the fluctuating velocity in the streamwise direction passes through a maximum. The location C is at the centre of the channel, where the mean velocity gradient as well as the amplitude of the fluctuating velocity are small. The location B is between these two.

The three important time scales in the problem are the viscous relaxation time for the particles, τ_v, the time between particle collisions, τ_c, and the correlation time for the fluid velocity fluctuations, which is the integral time τ_f. The present analysis is restricted to the parameter regime where τ_f is small compared to the collision and viscous relaxation time, so that the effect of fluid velocity fluctuations can be modelled as Gaussian white noise. We consider the fluid and particle velocity in the parameter regimes $\tau_v < \tau_c$, where the particle velocity equilibrates to the local fluid velocity between successive collisions, and $\tau_c < \tau_v$, where the time between collisions is smaller than the time required for the equilibration of the particle velocity with the local fluid velocity. A distinction can also be made between two different types of collisions, particle–particle and particle–wall collisions; the time between particle–particle collisions is denoted by $\tau_{c_{pp}}$, while that between particle–wall collisions is denoted $\tau_{c_{pw}}$. For dilute suspensions when $\tau_v < \tau_c$, two different cases may arise. The first is $\tau_v < \tau_{c_{pp}}$ and $\tau_v \sim$ or $> \tau_{c_{pw}}$, and in the other case τ_v is smaller than both $\tau_{c_{pp}}$ and $\tau_{c_{pw}}$. These cases were analysed separately in Goswami & Kumaran (2010*a*,*b*). However, it was found that there is not much difference in the statistics for the velocity and acceleration distributions for $\tau_v < \tau_{c_{pw}}$ and $\tau_v > \tau_{c_{pw}}$. Therefore, in the present analysis, we have examined only two regimes, the first at low volume fraction where $\tau_v < \tau_c$, and the other at larger volume fractions where $\tau_c < \tau_v$.

3.1. *Viscous relaxation time less than collision time*

In this subsection, we present the fluctuating particle velocity and acceleration distribution function (p.d.f.) for the case when the particle relaxation time is less than the inter-particle collision time. In the simulations, we have varied the viscous relaxation time by changing the particle density, and keeping the solid volume fraction (ϕ) equal to 9.4×10^{-5}. Figure 3(*a*) shows the normalized distribution functions of the streamwise particle velocity fluctuation at the central region (location C) of the channel for which $y^+ = 104.0$–115.5. The figure clearly shows a highly asymmetric and non-Gaussian distribution of the particle velocities, where there is a long nearly exponential tail in the negative velocity region. This indicates that there are a relatively small number of particles with velocity much larger than the mean velocity and a larger number with velocity less than the mean velocity. This is because the mean velocity is largest at the centre of the channel, and so particles that are transported to the centre from location B have a lower mean velocity than the mean velocity at the centre. Figure 3(*b*) shows the acceleration distribution functions for the particles in the same region. In this case, we observe a slowly decaying tail in the acceleration distribution for positive accelerations. This corresponds to the tail in the velocity distribution at negative velocities, which experience a positive acceleration due to the

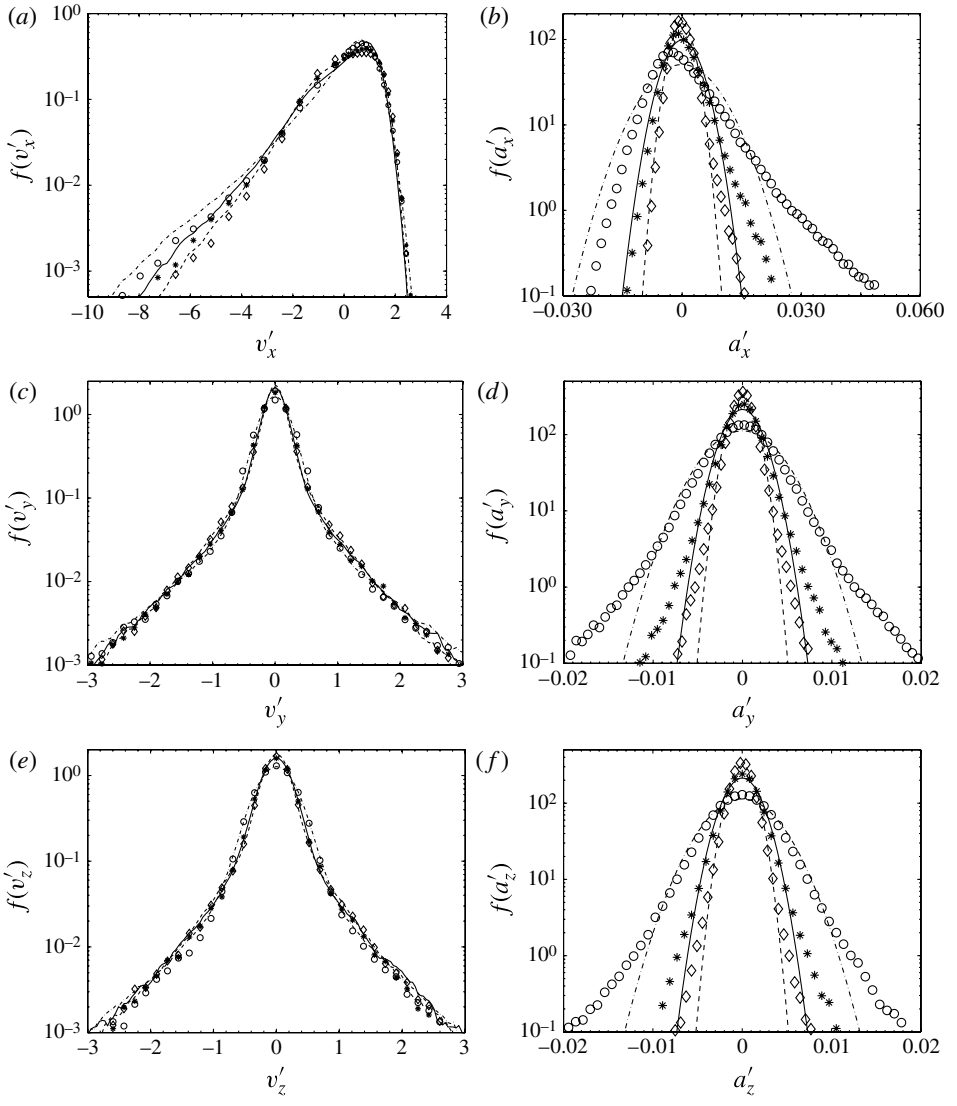

FIGURE 3. Components of particle velocity distribution function (a,c,e) and acceleration distribution function (b,d,f) at the centre of the channel ($y^+ = 104.0$–115.5), when viscous relaxation time of the particle is less than the particle–particle collision time, $\tau_v < \tau_{c_{pp}}$, and $\phi = 9.44 \times 10^{-5}$. Streamwise ($a$,$b$), wall-normal ($c$,$d$), and spanwise ($e$,$f$). DNS, run 1 ($\circ$); DNS, run 2 ($*$); DNS, run 3 ($\diamond$). In ($a$) fluctuating force simulation (FFS), run 1 (-·-); FFS, run 2 (—), and FFS, run 3 (− −). In (b,d,f) Gaussian fits for acceleration distributions are run 1 (-·-), run 2 (—), and run 3 (− −). Results of FFS are discussed in § 4.2. Parameters for all the runs are given in table 1.

difference between the mean velocity and the particle velocity. It is observed that the departure of the acceleration distribution from a Gaussian distribution is actually smaller than the departure of the velocity distribution from Gaussian.

Figure 3(c,d) shows the distribution functions for the wall-normal component of the particle velocity and acceleration. In contrast to the streamwise velocity distribution, the distribution of the wall-normal velocity fluctuations is symmetric, and it shows

very little variation with the viscous relaxation time of the particle. The velocity distribution shows very slow decay at higher values of fluctuations. As in the case of Couette flow, even when the velocity distribution is very different from Gaussian, the acceleration distribution is actually well described by a Gaussian distribution, even when the distribution function is 10^{-2} times its maximum value. This indicates that the slow decay of the particle velocity distribution is not due to a change in the form of the acceleration of the particles, but rather due to inter-particle collisions. For Couette flow (Goswami & Kumaran 2010*a*), it was observed that when the inter-particle collisions are switched off in the simulations, the slowly decaying tails in the velocity distribution disappear. A similar effect is observed in the present case of a channel flow, indicating that there are two distinct regimes in the velocity distribution in the transverse direction, one due to the fluid velocity fluctuation at low velocities, and the second due to inter-particle collisions, which results in relatively larger transverse velocities. The inter-particle collision effect is primarily due to the large anisotropy of the mean square of the fluctuating velocities. It should be noted from figure 3(*a–d*), that the mean square velocities and accelerations in the streamwise direction are significantly larger than those in the cross-stream direction. The particle velocity fluctuations in the streamwise direction induce collision between particles, and these collisions generate fluctuations in the wall-normal and spanwise directions. Such fluctuations result in highly non-Gaussian velocity distributions, even when the acceleration distribution is close to Gaussian. Identical conclusions can be drawn regarding the velocity and acceleration distributions in the spanwise direction from figure 3(*e*,*f*).

Next we analyse the effect of particle–particle collisions on mean acceleration and r.m.s. of the acceleration fluctuation. Since the collisions are instantaneous, the acceleration at a collision is infinite. So it is not possible to directly compare the average acceleration due to drag with that due to collisions. Since momentum is conserved in collisions, there is no net acceleration in a differential volume due to collisions. This is in contrast to fluid drag, where there is a net deceleration due to the drag force. The net momentum in a control volume could change only if a particle with its centre within the volume collides with one that has its centre outside, and thereby gains momentum. This momentum transfer process is subdominant in a dilute system, since the transport of momentum due to particle streaming (particle entering/leaving a differential volume) is large compared to collisional transport. The effect of collisions is best inferred by comparing simulation with and without collisions. In the latter case, one just permits the particles to go through each other, so that there are no collisions. The effect of collision is best inferred by comparing simulation with and without collisions. In the latter case, one just permits the particle to go through each other, so that there are no collisions. One such comparison is shown in figure 4.

It is found from figure 4(*a*) that acceleration near the wall is negative as particles move faster than the fluid, and positive at the centre of the channel as fluid velocity is higher than the particle velocity. The presence of collisions increases the particle velocity near the wall and decreases at the centre. Therefore the magnitude of acceleration increases near the wall and decreases at the channel centre in the presence of collisions. Figure 4(*b*,*c*) shows that collisions reduce the acceleration fluctuations in all three directions.

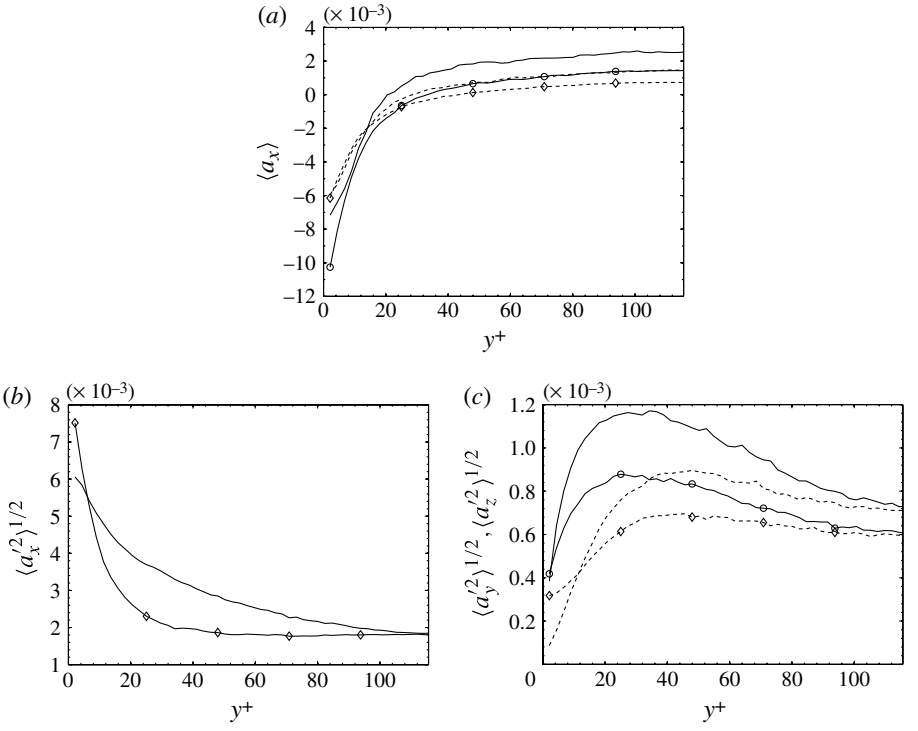

FIGURE 4. Mean and r.m.s. of particle acceleration in the presence and absence of particle–particle collisions across the width of the channel. (*a*) Mean particle acceleration, (*b*) r.m.s. of streamwise component of particle acceleration, and (*c*) r.m.s. of spanwise and cross-stream particle accelerations. (*a*) Run 2, without collisions (—); run 2, with collisions (—○); run 4, without collisions (− −); run 4, with collisions (− −◇). (*b*) Run 4, without collisions (—); run 4, with collisions (—◇). (*c*) $\langle a_z'^2\rangle^{1/2}$, run 4, without collisions (—); $\langle a_z'^2\rangle^{1/2}$, run 4, with collisions (—○); $\langle a_y'^2\rangle^{1/2}$, run 4, without collisions (− −); $\langle a_y'^2\rangle^{1/2}$, run 4, with collisions (− −◇).

3.2. *Collision time less than the viscous relaxation time*

In this section, we focus on the regime where particle–particle collision time, τ_c, is less than the viscous relaxation time, τ_v, of the particles. For all the simulations in this section, the volume fraction of the particles is $\phi = 7.0 \times 10^{-4}$, and the mass density of the particle has been changed to vary the relaxation time. The increase in viscous relaxation time τ_v increases the particle–particle collision time τ_c by reducing the mean square particle fluctuation (granular temperature), subject to the constraint $\tau_c < \tau_v$. Figure 5(*a*,*b*) shows the streamwise velocity distribution and acceleration distributions for different values of the viscous relaxation time at location C near the centre of the channel. In contrast to the regime $\tau_v < \tau_c$, we find here that the acceleration distribution in all directions is well described by a Gaussian distribution for a variation in the probability distribution of up to two decades even in the streamwise direction. The velocity distributions are also well approximated by a Gaussian distribution, though the agreement is not as good as that for the acceleration distribution. It is observed that, as expected, the Gaussian fit becomes better as the ratio of the viscous relaxation time and the collision time increases. Figures 5(*c*,*d*) and 5(*e*,*f*) show the wall normal and spanwise velocity and acceleration distribution

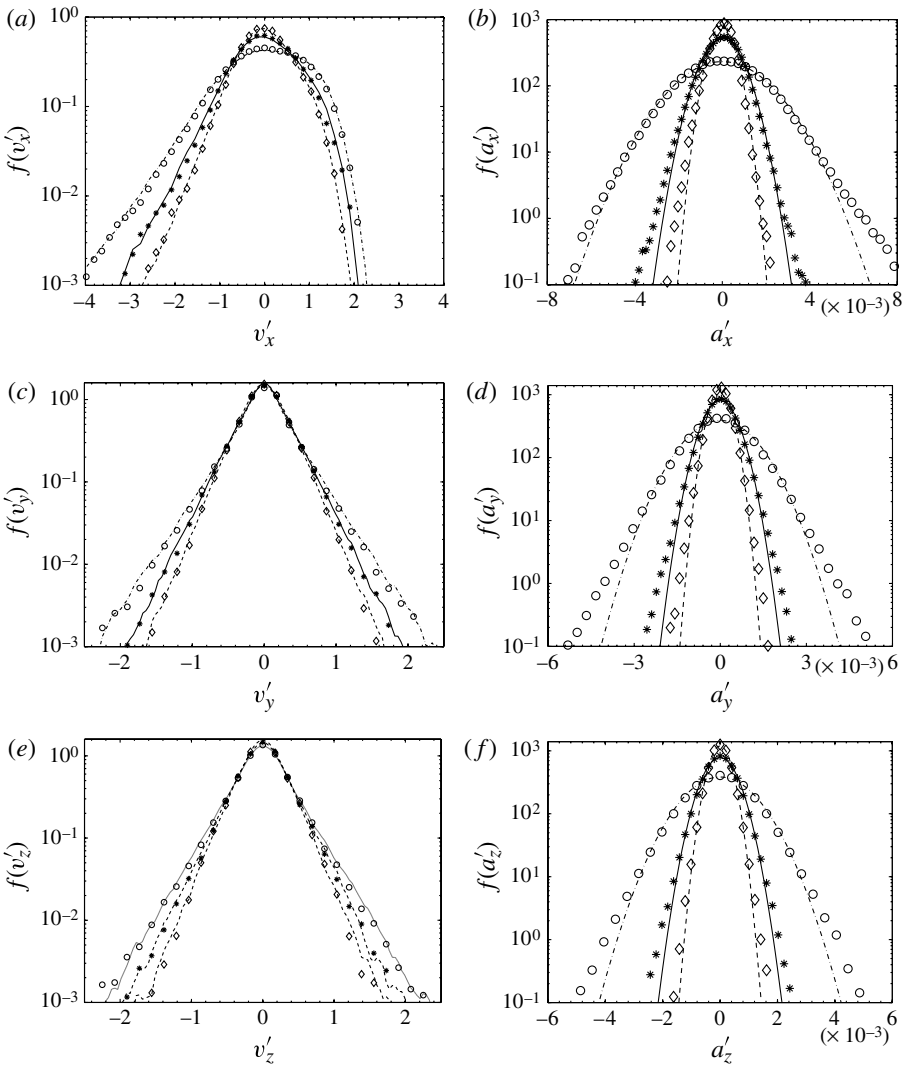

FIGURE 5. Components of particle velocity distribution function (*a*,*c*,*e*) and acceleration distribution function (*b*,*d*,*f*) at the centre of the channel ($y^+ = 104.0$–115.5), when particle–particle collision time is less than the viscous relaxation time of the particle, $\tau_{c_{pp}} < \tau_v$, and $\phi = 7.0 \times 10^{-4}$. Streamwise (*a*,*b*), wall-normal (*c*,*d*), and spanwise (*e*,*f*). DNS, run 5 (○); DNS, run 7 (∗); DNS, run 8 (◇). (*a*) FFS, run 5 (···); FFS, run 7 (—); FFS, run 8 (− −). (*b*,*d*,*f*) Gaussian fits for acceleration distributions are run 5 (···), run 7 (—), and run 8 (− −). Results of FFS are discussed in § 4.2. Parameters for all the runs are given in table 1.

functions. As in the streamwise case, we observe that the acceleration distribution is well described by a Gaussian distribution. The higher frequency of collisions reduces the anisotropy in the distribution of the fluctuating velocities. In addition to the greater collisional redistribution of energy, collisions also lead to a near-Gaussian velocity distribution.

The analysis of the particle acceleration distribution functions at different cross-stream positions for both regimes $\tau_v < \tau_c$ and $\tau_c < \tau_v$ indicates that the streamwise

component of the acceleration distribution at the centre of the channel shows the largest deviation from a Gaussian distribution, and the acceleration distributions in regions A and B are better approximated by a Gaussian distribution.

3.3. *Components of particle acceleration*

In this subsection, we focus on the acceleration of the particles, and examine separately the effect of the fluid velocity and the particle velocity fluctuations. The motivation for this detailed analysis is as follows. The results of the previous two subsections has shown that the particle velocity fluctuations and the particle acceleration fluctuations show large deviations from a Gaussian distribution, especially in the centre of the channel and in the regime $\tau_v < \tau_c$. There are three contributions to the acceleration of the particles: the first is due to the difference in the mean velocities of the particle and fluid, the second is the fluctuating velocity of the particles and the third is the fluctuating velocity of the fluid. The total acceleration is the sum of these three components. However, in the fluctuating force formulation, we approximate the acceleration due to fluid velocity fluctuations alone as random white noise with a Gaussian distribution. Therefore, the fluctuating force simulations will be accurate if the distribution of the fluid velocity fluctuations is close to a Gaussian distribution, even though the distribution of particle velocities may deviate significantly from a Gaussian distribution. Therefore, it is necessary to examine the distribution of the different components of the acceleration separately.

The centre region C of the channel is chosen for the analysis, since it shows the most interesting behaviour and the largest departure from a Gaussian distribution. The particle acceleration-fluctuation can be divided into two parts, the first due to the fluid velocity fluctuations, $\boldsymbol{u}'/\tau_v$, and the second due to the particle velocity fluctuations, $\boldsymbol{v}'/\tau_v$, in (3.2). We examine the distributions for each of these two separately. We also investigate the skewness and the flatness for particle acceleration due to fluid velocity fluctuation.

Figure 6 shows the p.d.f. for the acceleration due to fluid velocity fluctuation and the particle velocity fluctuation for the cases $\tau_v < \tau_c$, while figure 7 shows the acceleration distribution for $\tau_c < \tau_v$. In the regime $\tau_v < \tau_c$, from figure 6(*a*) it is observed that the acceleration due to particle velocity fluctuation has a long tail for the negative acceleration fluctuation, in contrast to the long tail for positive acceleration of the overall particle acceleration fluctuation. Both of these distributions deviate magnificently from the Gaussian distribution. However, the acceleration due to fluid velocity fluctuation is close to a Gaussian function, though it is slightly skewed to negative acceleration. This is consistent with the fluid velocity skewness reported by Dinavahi (1992) and Kim, Moin & Moser (1987), though it should be noted that their Reynolds number is, respectively, 2.5 and 1.5 times higher than that in the present study. In the wall-normal and spanwise directions, however, the acceleration due to the fluid velocity fluctuations is symmetric and Gaussian over a decrease in the distribution function of two orders of magnitude. The acceleration due to the particle velocity fluctuations is small compared to that due to the fluid velocity fluctuations, and the p.d.f. for the total acceleration is close to the p.d.f. for the acceleration due to fluid velocity fluctuations. Therefore, the total acceleration can be well approximated as a Gaussian function due to the fluid velocity fluctuations alone.

Figure 7 shows the p.d.f. for the acceleration distribution for the case where the time between collisions is small compared to the viscous relaxation time. In this case, we observe that the acceleration distribution function is a Gaussian function in all three directions. The component of the acceleration fluctuations due to the particle velocity

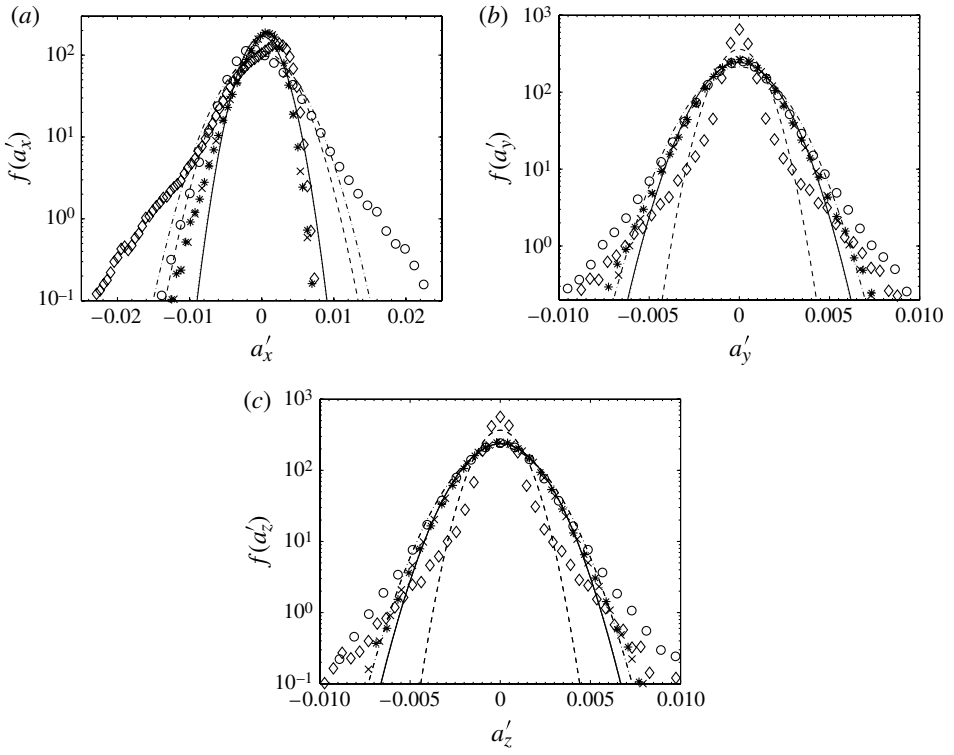

FIGURE 6. Streamwise (*a*), wall-normal (*b*), and spanwise (*c*) components of particle acceleration distribution function at the centre of the channel ($y^+ = 104.0$–115.5), calculated from the particle acceleration fluctuation, fluid velocity fluctuation at particle position, particle velocity fluctuation and fluid velocity fluctuation at the DNS grids within the specified y^+. In this case the viscous relaxation time of the particle is less than the particle–particle collision time, $\tau_v < \tau_c$, $\phi = 9.44 \times 10^{-5}$, simulation run 2. $f(a_i')$ ($\circ$), $f(u_i'/\tau_v)$ at particle positions ($*$), $f(v_i'/\tau_v)$ ($\diamond$), and $f(u_i'/\tau_v)$ at the fluid grid points ($\times$). The Gaussian fits are $f(a_i')$ (-··-), $f(u_i'/\tau_v)$ (—), $f(v_i'/\tau_v)$ (−−), and for $f(u_i'/\tau_v)$ at the fluid grid points (···). Parameters for run 2 are given in table 1.

fluctuations is small in all three directions, and the total acceleration is very close to the acceleration due to the fluid velocity fluctuations. In addition, the root mean square of the acceleration in the streamwise direction is only ∼45 % larger than that in the wall-normal and spanwise directions. This is in contrast to the case $\tau_v < \tau_c$, where it was observed that the root mean square of the acceleration fluctuations in the streamwise direction is about ∼2.5 times larger than that in the spanwise and wall-normal directions.

Another important distribution that is plotted in figures 6 and 7 is the distribution of the quantity $\boldsymbol{u}'/\tau_v$ in the fluid. While plotting the different components of the acceleration distributions, we had measured acceleration due to the fluid velocity fluctuations, $\boldsymbol{u}'/\tau_v$, and the acceleration due to the particle velocity fluctuations, $\boldsymbol{v}'/\tau_v$, in the simulation. Independently, we have also measured the distribution of $\boldsymbol{u}'/\tau_v$ in the fluid itself, and the distribution of this is plotted in figures 6 and 7. It is observed that there is very good agreement between the distributions for $\boldsymbol{u}'/\tau_v$ at the particle positions and that in the fluid, indicating that there is no correlation between the particle and fluid velocities at the Stokes number considered here. A similar feature

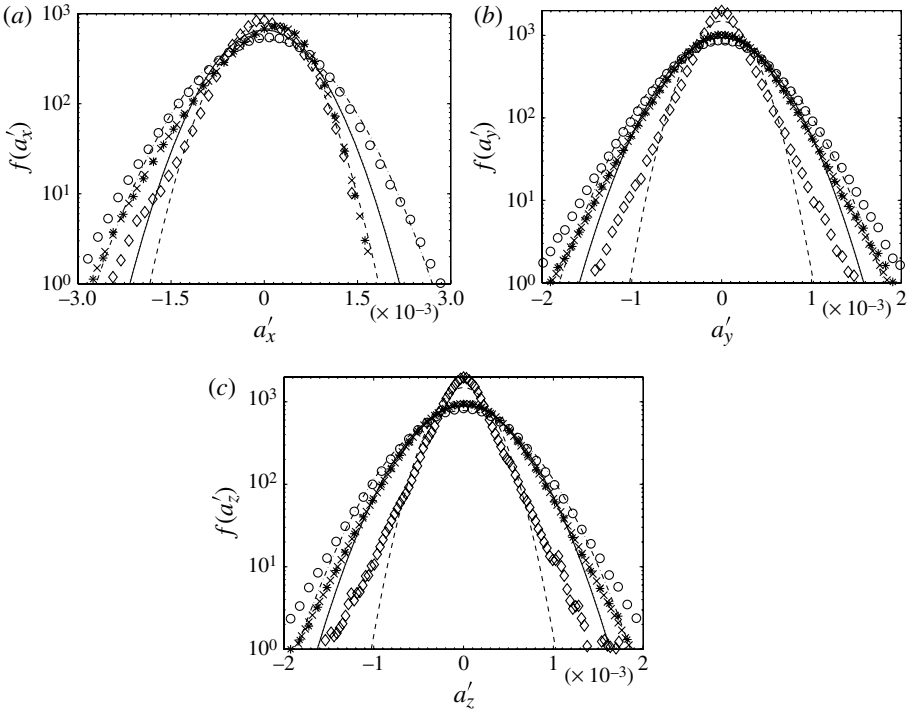

FIGURE 7. Streamwise (a), wall-normal (b), and spanwise (c) components of particle acceleration distribution functions at the centre of the channel ($y^+ = 104.0$–115.5), calculated from the particle acceleration fluctuation, fluid velocity fluctuation at particle position, particle velocity fluctuation and fluid velocity fluctuation at the DNS grids within the specified y^+. In this case the particle–particle collision time is less than the viscous relaxation time of the particle, $\tau_c < \tau_v$, $\phi = 7.0 \times 10^{-4}$, simulation run 7. $f(a_i')$ ($\circ$), $f(u_i'/\tau_v)$ at particle positions ($*$), $f(v_i'/\tau_v)$ ($\diamond$), and $f(u_i'/\tau_v)$ at the fluid grid points ($\times$). The Gaussian fits are $f(a_i')$ (-·-), $f(u_i'/\tau_v)$ (—), $f(v_i'/\tau_v)$ (– –), and for $f(u_i'/\tau_v)$ at the fluid grid points (···). Parameters for run 7 are given in table 1.

was also observed in Couette flow in Goswami & Kumaran (2010*a*). Therefore, the acceleration distribution function can be estimated from the distribution of the fluid fluctuating velocities. It should be noted that our calculation is limited to the case of one-way coupling, where the effect of the particles on the fluid velocity is not taken into account. It is necessary to carry out further studies to examine the effect of particle forcing on the correlation between the fluid and particle velocities.

In order to quantify the departure from a Gaussian distribution, we have also calculated the skewness and flatness of the particle acceleration due to fluid velocity fluctuation for both the regimes. For the velocity distribution, the skewness and flatness are defined by

$$\text{skewness} = \frac{\langle v_i'^3 \rangle}{(\langle v_i'^2 \rangle)^{3/2}}, \tag{3.3}$$

$$\text{flatness} = \frac{(\langle v_i'^4 \rangle - 3(\langle v_i'^2 \rangle)^2)}{(\langle v_i'^2 \rangle)^2}. \tag{3.4}$$

A similar definition is used for the acceleration distribution.

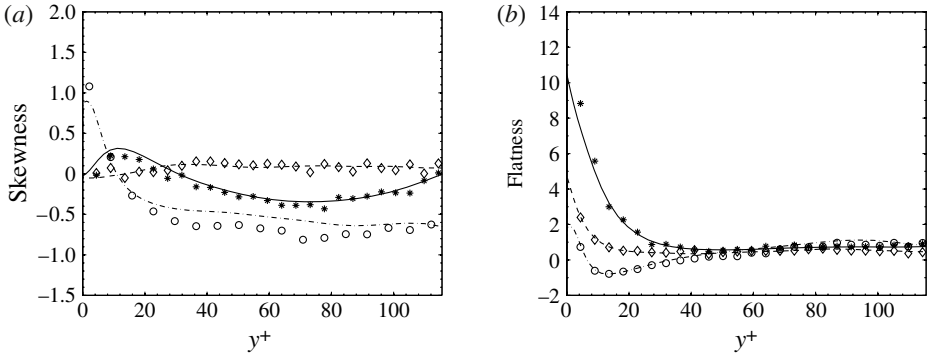

FIGURE 8. Skewness (*a*) and flatness (*b*) of the fluctuating particle acceleration which originates from the fluid velocity fluctuation for $\tau_v < \tau_{c_{pp}}$, and simulation run 2. The components of particle acceleration are streamwise (○), wall-normal (∗), and spanwise (◇). The fluid velocity fluctuations are streamwise (-··-), wall-normal (—), and spanwise (− −).

For the case $\tau_v < \tau_c$, both the skewness of fluid velocity fluctuation and the streamwise particle acceleration are negative across nearly 80 % of the channel width (figure 8). This is due to the long tail in the acceleration distribution for negative accelerations in figure 6. The skewness of the streamwise acceleration due to the particle velocity fluctuations becomes positive near the wall, but it is nearly zero at the point where the root mean square of the fluid fluctuating velocity is a maximum. The skewness in the cross-stream direction is numerically smaller than that in the streamwise direction. The skewness in the spanwise direction is zero across the channel, as required by symmetry. The flatness in the distribution is small near the centre of the channel, but becomes large only near the walls. The results for the regime $\tau_c < \tau_v$ are nearly identical to that shown in figure 8. This is expected due to a combination of two effects. Firstly, we have only one-way coupling in the present simulations, and the presence of particles does not affect the fluid velocity fluctuations. Secondly, the analysis of the different components of the acceleration distribution has shown that the acceleration due to the fluid velocity fluctuations is identical to that calculated from the fluid velocity fluctuations in the absence of particles, indicating that there is no correlation between the particle and fluid fluctuations. Due to this, the distributions of the acceleration due to fluid velocity fluctuations should be unaffected by the presence of the particles. We have verified, in simulations, that this is true, and the acceleration distribution due to fluid velocity fluctuations is unaffected by the ratio of the viscous relaxation time and the collision time. For simplicity, we consider the distribution of the particle acceleration due to fluid velocity fluctuations to be Gaussian. Figure 8 shows that the maximum departure from the Gaussian distribution is near the walls of the channel. Despite this, we get reasonably good agreement between the DNS and the fluctuating force simulations even near the walls when the viscous relaxation time is smaller than the collision time, as shown in § 3. This is probably because the amplitude of the fluid velocity fluctuations decreases as the wall is approached, and the dominant contribution to the particle velocity fluctuations is the inter-particle collisions induced by the mean shear.

3.4. *Acceleration correlation function*

The time correlation of the particle acceleration is an issue of importance in the modelling of the effect of turbulent fluctuations on the particle phase (Goswami &

Kumaran 2010*a*). The time correlation function of the particle acceleration has been computed and compared with the time correlation for the fluid velocity fluctuations.

It is necessary to define, carefully, the procedures used for calculating the fluid velocity and the particle acceleration correlations. It should be noted that the objective of the present analysis is to propose a fluctuating force model for the effect of turbulent flow on the particles, and to calculate the moments of the force distribution which correctly reproduces the effect of the fluid on the particles. The moments are obtained from the time integrals of the velocity autocorrelation functions, and it is an issue of importance to determine how the autocorrelation function should be calculated. In Goswami & Kumaran (2010*a*,*b*), the autocorrelation functions were calculated over the central 20 % of the Couette flow, where the mean velocity passes through zero. Therefore, there was no difference in the autocorrelation functions in a fixed reference frame and that in a reference frame moving with the mean fluid velocity. In the present case, the mean velocity is at a maximum at the centre of the channel, and so it is necessary to determine the correct procedure for calculating the autocorrelation function. We have computed the time correlation for the fluid velocity fluctuation in two different reference frames; the first is the fixed Eulerian reference frame at a given location in space, and the second is a 'moving Eulerian' reference frame, where the location of the measurement of fluid velocity fluctuation moves with the mean velocity of the fluid. The acceleration correlation on the particles is calculated in a Lagrangian reference frame moving with the particles. A comparison of the correlation times has been used to determine the correct variances of the force distributions to be used in the Langevin description.

The acceleration correlation coefficient is given by

$$R_{aa}(\tau) = \frac{\langle \boldsymbol{a}'(t) \cdot \boldsymbol{a}'(t+\tau) \rangle}{\langle \boldsymbol{a}'(t) \cdot \boldsymbol{a}'(t) \rangle}. \tag{3.5}$$

Here, the accelerations at different times have been calculated in a reference frame moving with the particle, and the angular brackets in the above equation represents an average over a large number of particles. The fluctuation of the acceleration has been calculated by subtracting the local average of the acceleration from instantaneous acceleration of the particle.

Figure 9(*a–c*) shows the acceleration correlation coefficient as a function of time for the case when particle relaxation time is less than the particle–particle collision time. For clarity, we have cut off the time axis at a non-dimensional time of 100. The long time integration of the acceleration correlation function provides the acceleration correlation time of the particle, proportional to the Lagrangian fluid time scale in a reference frame moving with the particle, provided that the main contribution to the particle acceleration fluctuation is the fluid velocity fluctuation. It is observed that the correlation of fluid velocity fluctuation in a fixed Eulerian reference frame decays much faster than that in a moving Eulerian reference frame, but the latter decays at a similar rate to that of the correlation of particle acceleration fluctuation. This is because of the convection of eddies across a location due to the mean velocity, which results in a faster decorrelation in a fixed Eulerian reference frame. It is clearly observed that there is good agreement between the acceleration correlation function and the fluid correlation function in a moving Eulerian reference frame moving with the mean velocity of the fluid. It is important to note that the moving Eulerian reference frame is different from a Lagrangian reference frame moving with the fluid velocity.

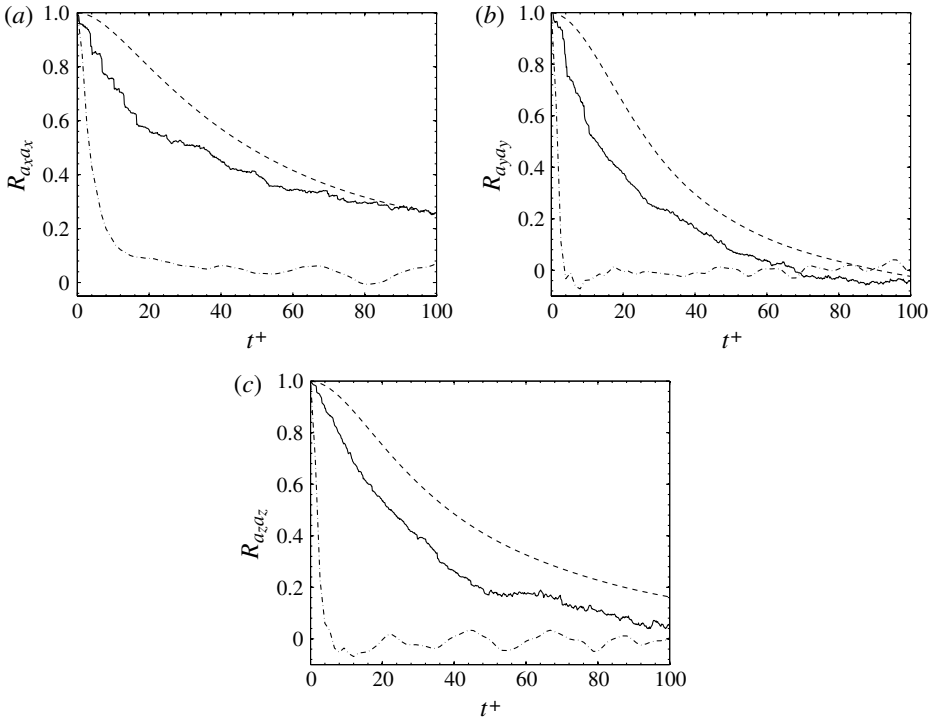

FIGURE 9. Time correlation of the fluid velocity fluctuations and particle acceleration fluctuations at the centre of the channel. For particle acceleration correlation $y^+ = 104.0$–115.5 and simulation run 1, and for fluid velocity correlation $y^+ = 104.0$. The plots are fluid velocity correlation in the fixed Eulerian frame (---), in the moving Eulerian frame (——), and particle acceleration correlation (—) for streamwise (*a*), wall-normal (*b*) and spanwise (*c*) components of fluid velocities and particle accelerations. All the parameters for run 2 are given in table 1.

Since the flow is highly inhomogeneous in the wall-normal direction, verification of the comparability of the particle acceleration correlation time with the fluid velocity correlation time at different cross-stream positions becomes an important issue. Particle acceleration correlation coefficients have been calculated in each of the three cross-stream positions A, B and C (figure 2). The particle acceleration correlation time, which is obtained from the time integration of the correlation coefficient, has been calculated by considering 10 ensembles of 200 particles each. During the simulation, we separately consider the particles that are located in the different wall-normal regions of the channel (positions A, B and C in figure 2 of the article). If a particle moves out of a particular region due to its transverse motion at any instant, this particle is not included in the correlation calculation for later times. For each ensemble, we have considered the trajectories of at least 200 particles. When the particle number in the region becomes less than 200, we stop the sampling. Averaging is carried out over 10 such ensembles to determine the correlation time. The acceleration correlation time is calculated along with the fluid velocity correlation time in both the fixed Eulerian and moving Eulerian reference frame at the different cross-stream positions A, B and C (figure 2). The calculation shows that the acceleration correlation times are of the same order of magnitude as the Eulerian velocity autocorrelation time in the

Cross-stream positions	Particle acceleration correlation time			Fluid velocity correlation time in a moving Eulerian frame			Fluid velocity correlation time in fixed Eulerian frame		
	τ_x^a (% std dev.)	τ_y^a (% std dev.)	τ_z^a (% std dev.)	τ_x	τ_y	τ_z	τ_x	τ_y	τ_z
A	81.9 (1.9)	9.1 (13.7)	27.6 (13.7)	52.7	19.5	21.8	13.0	5.0	4.5
B	71.5 (6.2)	19.4 (5.2)	23.8 (10.9)	61.7	29.3	33.8	10.6	3.8	2.5
C	69.2 (2.5)	23.4 (12.8)	33.5 (15.2)	51.3	21.5	23.0	8.2	1.2	1.2

TABLE 2. Particle acceleration correlation time and fluid velocity time scale at three positions across the channel.

moving Eulerian frame, but larger than that in the fixed Eulerian frame, at all locations as shown in table 2.

From figure 9, it is clear that the acceleration correlation time is largest in the streamwise direction, while it is lower in the wall-normal and spanwise directions. The acceleration correlation time does not show much variation when the ratio of the viscous relaxation time and collision time is changed, and it is of the same order of magnitude as the Eulerian velocity autocorrelation time (integral time). More importantly, this acceleration correlation time is much smaller than both the viscous relaxation time and the time between collisions for the Reynolds numbers and the Stokes numbers considered here. This implies that the acceleration of the particles due to the fluid velocity fluctuations can be well represented by Gaussian white noise, over time scales comparable to the viscous relaxation time or the collision time. However, it should be noted that the noise has to be highly anisotropic, since the magnitude of the fluid velocity fluctuations in the flow direction is significantly larger than that in the cross-stream and spanwise directions.

The good correlation between the acceleration correlation function and the fluid velocity correlation function in a moving Eulerian reference frame can be explained as follows. There are two issues to be noted with regard to the parameter regime being considered here. The first is that in the high-Stokes-number regime, particle inertia is large and so particles do not follow the fluid streamlines. Therefore, the relaxation of fluid velocity fluctuations along fluid streamlines is not relevant for the particle acceleration. Secondly, when the viscous relaxation time is small compared to the time between collisions, the particles relax locally to the fluid mean velocity. Therefore, it is sufficient to consider the fluid velocity correlation function in a reference frame moving with the local fluid velocity. However, it should be noted that the above approximation is a good one only when the slip between the fluid and particle phases is relatively small. When the slip is substantial, the particle mean velocity cannot be well approximated by the fluid mean velocity, and so the acceleration correlation time cannot be calculated from the fluid velocity correlation time in a moving Eulerian reference frame. This issue has been addressed further in § 4.1.

4. Fluctuating force simulation

Here, we briefly describe the theory and the simulation procedure for the fluctuating force simulation, which was discussed in detail in Goswami & Kumaran (2010*b*).

The Boltzmann equation for the particle velocity distribution function, for a two-dimensional flow with velocity in the x direction and velocity gradient in the y direction, can be expressed as

$$\frac{\partial f(\boldsymbol{v}')}{\partial t} + (\bar{v}_i + v_i')\frac{\partial f(\boldsymbol{v}')}{\partial x_i} - \dot{\gamma}\frac{\partial v_y' f(\boldsymbol{v}')}{\partial v_x'} - \frac{1}{\tau_v}\frac{\partial((v_i' + \bar{v}_i - \bar{u}_i)f(\boldsymbol{v}'))}{\partial v_i'} - D_{ij}\frac{\partial^2 f(\boldsymbol{v}')}{\partial v_i' \partial v_j'} = \frac{\partial_c f(\boldsymbol{v}')}{\partial t}, \tag{4.1}$$

where $f(\boldsymbol{v}')$ is the particle velocity distribution function, defined such that $f(\boldsymbol{v}')\mathrm{d}\boldsymbol{v}$ is the probability of finding a particle in the volume $\mathrm{d}\boldsymbol{v}'$ about $\boldsymbol{v}'$ in the velocity space. Here, it is important to note that $\boldsymbol{v}'$ is the particle fluctuating velocity. The particle instantaneous velocity is $v_i' + \bar{v}_i(y)$, where $\bar{v}_i(y)$ is the mean velocity parallel to the streamwise direction, which is a function of the cross-stream coordinate y. The first term on the left-hand side of (4.1) is the rate of change of distribution function with time, the second term is the rate of change of the distribution function due to particle motion, and the third term is the change in the distribution function due to mean shear on the particles, where $\dot{\gamma} = \mathrm{d}\bar{v}/\mathrm{d}y$ is the mean strain rate. The fourth term represents the effect of drag force on the particles, where τ_v is the viscous relaxation time of the particle. The fifth term is the change in distribution function due to fluctuating gas velocity modelled as Gaussian random noise. The term on the right-hand side of (4.1) is the rate of change of the distribution function due to particle collisions, and is called the 'collision integral':

$$\frac{\partial_c f(\boldsymbol{v}')}{\partial t} = \rho\chi(\phi)\int \mathrm{d}\boldsymbol{k}\int \mathrm{d}\boldsymbol{v}'^{*}(f(\boldsymbol{v}_b')f(\boldsymbol{v}_b'^{*}) - f(\boldsymbol{v}')f(\boldsymbol{v}'^{*}))\boldsymbol{w}\cdot\boldsymbol{k}. \tag{4.2}$$

In (4.2), $\boldsymbol{v}_b'$ and $\boldsymbol{v}_b'^{*}$ are the velocities of the pair of particles before the collision, and $\boldsymbol{v}'$ and $\boldsymbol{v}'^{*}$ are the post-collision velocities, $\boldsymbol{k}$ is the unit vector in the direction of the line joining the centres of the colliding particles, $\boldsymbol{w} = \boldsymbol{v}' - \boldsymbol{v}'^{*}$ is the difference in velocity of the particles, $\chi(\phi)$ is the pair distribution function, which is 1 in the limit of low volume fractions analysed here. The integral in (4.2) is carried out for the condition $\boldsymbol{w}\cdot\boldsymbol{k} \geqslant 0$, so that the particles approach each other before the collision. Further details of the fluctuating force model is given in the Appendix.

4.1. *Simulation technique*

The configuration and coordinate system is the same as that in figure 1. The fluctuating force simulations have been carried out using a variable-time-step molecular dynamics procedure, and the time step for advancement is less than the integral time scale of the fluid. We have seen in the § 3.3 that the acceleration distribution on the particles due to the fluid velocity fluctuations can be accurately captured from the distribution of fluid velocity fluctuations in an Eulerian reference frame moving with the mean velocity of the fluid. This is because, as described in § 3.4, the integral time calculated in a reference frame moving with the local mean air velocity is closer to the particle acceleration correlation time, whereas the fluid integral time scale obtained in the fixed Eulerian reference frame is very different. It would be more exact to calculate the diffusion coefficients in a reference frame moving with the mean velocity of the particles, since we are considering the correlation of the acceleration of the particles. To examine if the difference in the fluid and the particle mean velocities cause a substantial variation in the correlation time, we have compared the integral times in two moving Eulerian reference frames, one moving

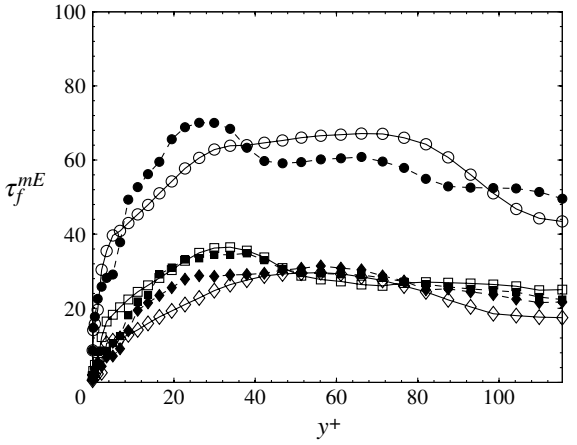

FIGURE 10. Fluid integral time scale in a reference frame moving with local fluid mean velocity (filled symbols) and with particle average velocity (open symbols). The particle relaxation time $\tau_v = 1351.1$. The components of the time scale are streamwise ∘, spanwise □, and wall-normal ◇.

with the local mean velocity of the fluid and the other moving with the local mean velocity of the particles. The result is shown in figure 10. We find that the maximum difference in time scale is 15 % if the velocity of the reference frame is either the air velocity or the particle velocity. There are errors in the correlation time estimates near the wall due to the difference in velocities between the particle and fluid phase. However, the diffusivities themselves decrease to zero at the wall, because the fluid velocity fluctuations decrease to zero. The dominant contribution to particle velocity fluctuations near the wall is due to the mean fluid shear and the cross-stream migration of the particles. Therefore, the error in the diffusivities do not have a significant effect on the particle dynamics near the wall. This indicates that we can obtain a good approximation for the diffusion coefficients by calculating the correlation functions in a reference frame moving with the mean fluid velocity. This is a significant simplification, since the fluid velocity is known *a priori* from the direct numerical simulations when we use one-way coupling, whereas the particle mean velocity has to be calculated by solving the equations for the particle phase using the fluctuating velocity in the fluid. Therefore, in order to determine components of D_{ij}, we estimate the autocorrelation in a moving Eulerian reference frame moving with the same mean velocity as the fluid.

The second moments for the random force distributions are calculated from the velocity autocorrelation function for the fluid fluctuating velocity in a moving Eulerian reference frame in the absence of the particles, and using

$$D_{ij} = \frac{\langle u_i'(0)u_j'(0)\rangle}{\tau_v^2}\int_0^\infty \mathrm{d}t' \frac{\langle u_i'(t')u_j'(0)\rangle}{\langle u_i'(0)u_j'(0)\rangle} = \frac{\langle u_i'(0)u_j'(0)\rangle}{\tau_v^2}\int_0^\infty \mathrm{d}t' R_{ij}, \tag{4.3}$$

where R_{ij} is the Eulerian time correlation tensor of the turbulent flow field. From the direct numerical simulation, we can calculate the Eulerian time correlation function in a moving Eulerian reference frame. The non-zero components of the diffusion tensor,

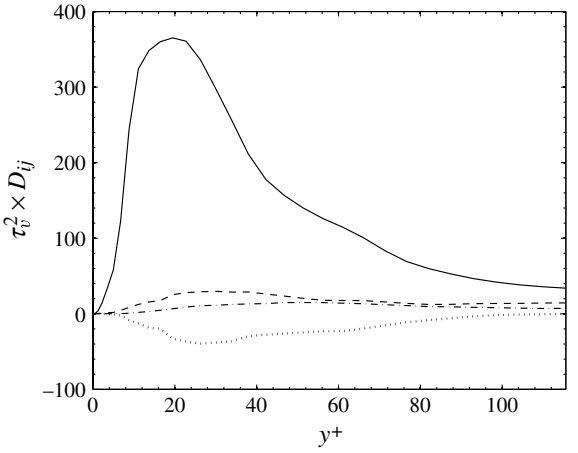

FIGURE 11. Velocity space diffusion coefficient across the width of the channel: D_{xx} (—), D_{yy} (·-·), D_{zz} (– –), D_{xy} (···).

obtained using (4.3), have been shown to be functions of the wall-normal coordinate in figure 11.

The simulation is initiated with a random initial configuration of the particles. At each step, we calculate the fluid drag on the particle which is generated due to the difference in particle instantaneous velocity and the local average fluid velocity; the latter is obtained from the results of the DNS channel flow simulation in the absence of the particles. We use cubic spline interpolation in the wall-normal direction to obtain the average fluid velocity at the particle position. Particle collisions are implemented using the usual collision rules between spherical elastic particles, where the relative velocity along the line joining the centres is reversed in a collision, while the relative velocity perpendicular to the line joining the centres remains unchanged. Impending particle collisions are predicted by a deterministic method, as done in the case of DNS, and not using the type of stochastic procedure used in direct simulation Monte Carlo. We consider only binary collisions, because the probability of multi-body collision is small at low volume fractions. To make the collision prediction more computationally efficient, we divide the simulation domain into three-dimensional lattice cells, and then we find the collision time for each particle by scanning potential collision partners from the same cell, or from a neighbouring cell. We have used 15^3 lattice cells with an average of 2–3 particles per cell. The updating of the particle velocity is done in accordance with (A 3), with the random noise chosen in accordance with (A 6). At every step, we calculate the drag on the particle, which depends on its wall-normal position. If a collision occurs within the simulation time step Δt, we advance all the particles in position and velocities by the time Δt_c up to the collision time. After each collision the post-collision velocities of the colliding particles are calculated, as described in Goswami & Kumaran (2010*b*). The parameters used for the simulations are given in table 1.

4.2. *Results of the fluctuating force simulation*

The results of the fluctuating force simulations are now compared with the results of the direct numerical simulations for a suspension with different $\tau_v < \tau_c$ and $\tau_c < \tau_v$. First, we compare the mean velocity profiles, the concentration profiles, and the root

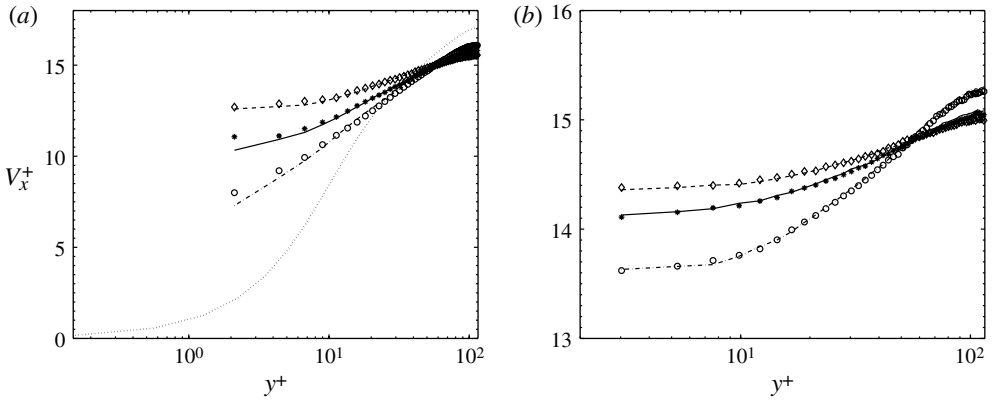

FIGURE 12. Streamwise mean velocity of the particle phase for different particle relaxation times $\tau_v < \tau_{cpp}$ (*a*) and $\tau_{cpp} < \tau_v$ (*b*). (*a*) Simulation run 1, DNS (○); run 2, DNS (∗); run 4, DNS (◇); run 1, FFS (-·-); run 2, FFS (—); run 3, FFS (− −); and air velocity profile (···). (*b*) Simulation run 5, DNS (○); run 7, DNS (∗); run 8, DNS (◇); run 5, FFS (-·-); run 7, FFS (—); run 8, FFS (− −). Parameters for all the runs are given in table 1.

mean square fluctuating velocities of the particles across the width of the channel. The second is a comparison of the velocity distributions from the fluctuating force and the direct numerical simulations, in order to determine whether the non-Gaussian nature of the velocity distribution functions can be obtained using a Gaussian acceleration distribution function. The fluctuating force simulations are run for a time period 3–5 times τ_v, required for steady state to be achieved. Then, we carry out the sampling for a duration of three times τ_v.

First, we consider the flow for a volume fraction of 9.44×10^{-5}, where the viscous relaxation time is small compared to the time between particle–particle collisions. Figure 12(*a*) shows the mean streamwise particle velocities at different wall-normal positions of the channel for three different values of the particle relaxation time. A salient feature of these mean velocity profiles is the significant difference between the particle and fluid mean velocities near the wall. Figure 13 shows the mean slip velocity scaled with the Stokes terminal velocity, v_{ts}^+, of the particles at different wall-normal positions. The slip velocity is positive near the wall, where particles move faster than air, and it is negative at the centre, where the particles move slower than the fluid. From figure 12, it is also clear that locally, the magnitude of the slip velocity is much larger than the Stokes terminal velocity of the particles in all cases. This indicates that the gravitational force on the particles is small compared to the drag force due to the difference in the mean velocity between the fluid and the particles locally. However, the two have to balance when integrated over the channel cross-section from force balance, since there is no force exerted by the sidewalls due to the elastic collision law assumed. For this reason, the slip velocity is positive near the wall and negative at the centre, in such a way that the macroscopic streamwise force balance on the particle phase is satisfied.

It should be cautioned that the relative magnitude of the gravitational force and the drag force depends on the fluid mean velocity. This ratio is small in the present configuration, because we have considered a channel of width ∼3–4 mm, so that a quantitative comparison can be made between the DNS and the fluctuating force simulations. Since the channel width is significantly smaller than that in practical

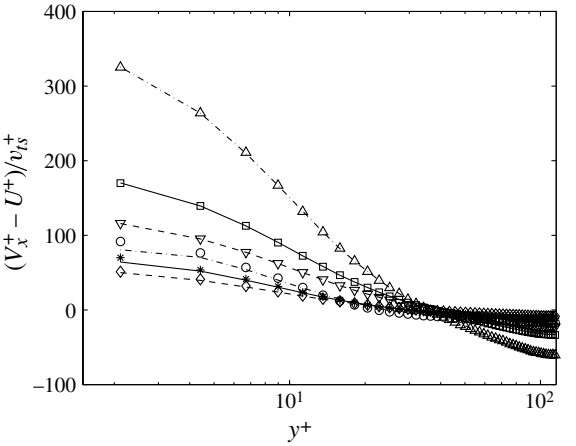

FIGURE 13. Slip velocity of the particle at different cross-stream positions of the channel for the cases $\tau_v < \tau_{c_{pp}}$ and $\tau_{c_{pp}} < \tau_v$. Simulation run 1, DNS (○); run 2, DNS (∗); run 4, DNS (◇); run 1 , FFS (-··-); run 2, FFS (—); run 4, FFS (− −); run 5, DNS (△); run 7, DNS (□), run 8, DNS (▽); run 5, FFS, (-··-); run 7, FFS (—); run 8, FFS (− −). Parameters for all the runs are given in table 1.

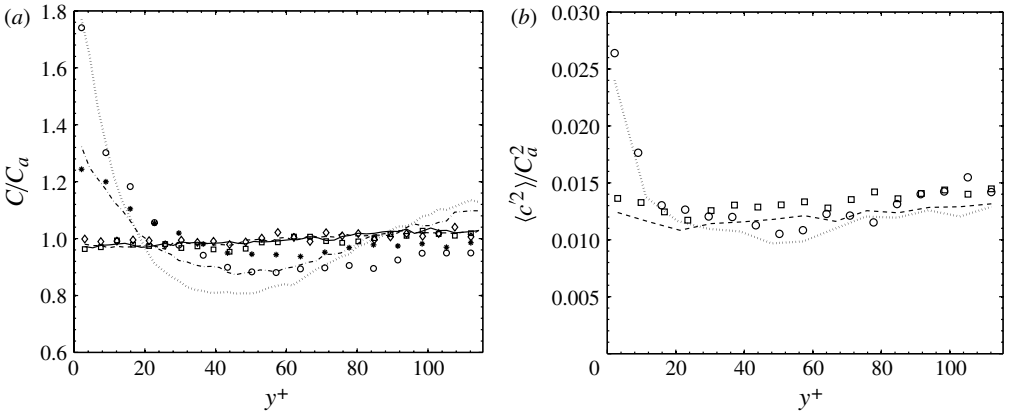

FIGURE 14. Variation of normalized particle concentration (*a*) and mean square of the particle concentration fluctuation (*b*) at different cross-stream positions in the channel for the cases $\tau_v < \tau_{c_{pp}}$ and $\tau_{c_{pp}} < \tau_v$. Simulation run 1, DNS (○); run 2, DNS (∗); run 1, FFS (···); run 2, FFS (-··-); run 5, DNS (□); run 7, DNS (◇); run 5, FFS (− −); run 7, FFS (—). Parameters for all the runs are given in table 1. For clarity in (*b*) we have shown results for run 1 and run 5 only.

applications, the fluid velocity is much larger at a fixed Reynolds number. Due to this, the ratio of the Stokes terminal velocity and the fluid velocity is small.

The variation in normalized particle concentration and fluctuation in particle concentration are shown in figure 14(*a,b*), where the normalization has been done with respect to the average particle concentration across the channel. The particle concentration profile shows that there is a migration of the particles towards the wall of the channel at lower particle relaxation time; this is because of the inhomogeneity in the fluctuating force exerted on the particles. Since the mean square of the fluctuating force (due to the fluid velocity fluctuations) in the wall-normal direction is lower near the wall of the channel when compared to the centre, there is a diffusion of

particles towards the wall. In the case of the velocity profile, it is observed that there is quantitative agreement between the DNS and fluctuating force simulations, even though the relaxation time is only about three times the fluid integral time scale. In the case of the concentration profile, there is a maximum difference of $\sim 18\,\%$ for the lowest viscous relaxation time. Moreover, the concentration profile for fluctuating force simulation shows a non-monotonic variation of concentration with y^+. This correlates with the diffusion coefficient data (figure 11), where the cross-stream diffusion coefficient is highest at position B, and decreases from there both to the centre and walls. Due to the cross-stream diffusion, particles diffuse from position B both to the centre and the walls, resulting in a concentration minimum in the region B. The concentration at the wall increases because the cross-stream diffusivity there goes to zero. The difference between the DNS and FFS results is possibly because the particle relaxation time is only about three times larger than the fluid relaxation time for run 1 (this has the lowest particle relaxation time). Figure 14(*b*) shows a variation of mean square of the concentration fluctuation, $\langle c'^2 \rangle / C^2$, where c' is the difference between the instantaneous and the average concentration at each location, and the average is taken over time. It is clearly observed that the root mean square of the concentration fluctuations is small compared to the mean concentration in this case. The concentration fluctuations increase as the wall is approached, and this increase is captured by the fluctuating force simulations.

Figure 15 shows the variation of the second moments of the particle velocity distributions across the channel. Figure 15(*a*) shows that the mean square velocities in the flow direction are quantitatively predicted by the fluctuating force simulations. The streamwise mean square velocities increase as the wall is approached, for two reasons. The first is the increase in the velocity gradient as the wall is approached, which results in greater fluctuations due to the cross-stream motion of the particles. The second is that the mean square of the fluid velocity fluctuations also exhibit maxima near the wall of the channel, as shown in figure 2. It should be noted that the particle–wall collisions are considered to be elastic and smooth, so that particle–wall collisions do not result in fluctuations in the streamwise direction.

The second moment of the velocity distribution $\langle v_x' v_y' \rangle$, which is also the particle phase streaming stress, is also quantitatively predicted by the fluctuating force simulations. This stress has to go to zero at the wall (figure 15*d*) for the particle–wall collision model we have chosen, because particle–wall collisions are elastic and smooth, and they do not exert any net stress on the particles. The mean square velocities in the wall-normal and spanwise directions (figure 15*b*,*c*) are also in good agreement, though the difference (the maximum difference is $\sim 25\,\%$) is larger than that in the streamwise direction (the maximum difference is $< 5\,\%$). It should be noted that the mean square velocities in the wall-normal and spanwise directions are numerically smaller than those in the streamwise direction in both DNS and FFS; this could be the reason for the poorer agreement.

Finally, we note that the agreement between the fluctuating force simulation and direct numerical simulation is relatively poor for the lowest viscous relaxation time used here, which is only about three times the correlation time for the fluid velocity fluctuations. The agreement gets much better as the viscous relaxation time is increased. This is expected, because a Langevin formulation is applicable only when the fluid velocity correlation time is small compared to that for the particle relaxation time. The results here indicate that the viscous relaxation time has to be at least about five times greater than the fluid velocity correlation time for the present model to provide accurate results.

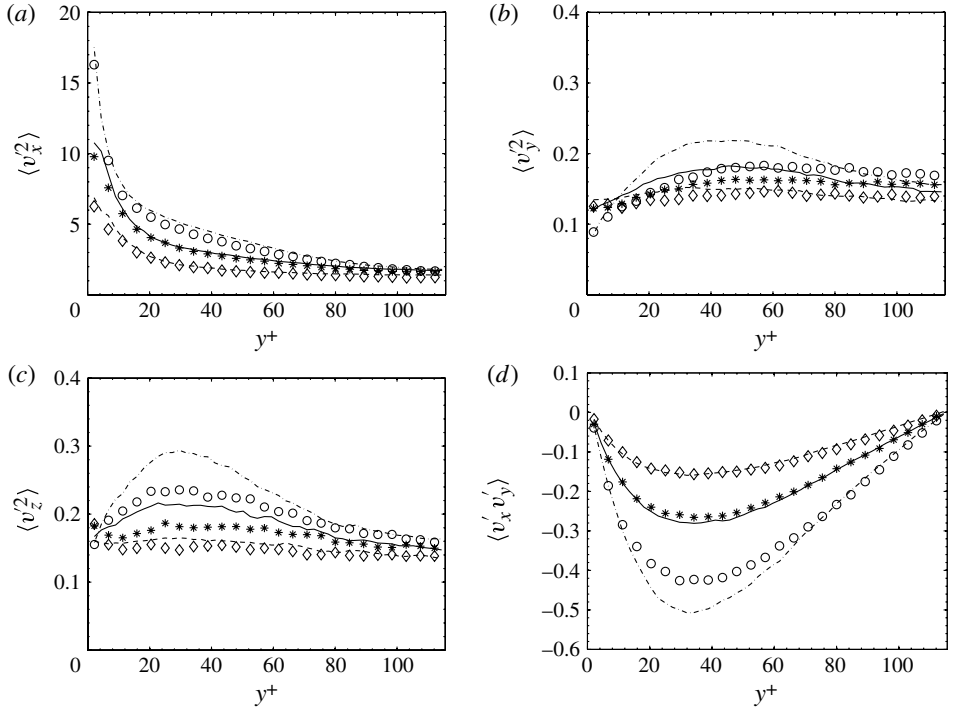

FIGURE 15. Variation of the second moments of the particle velocity distribution $\langle v_x'^2 \rangle$ (*a*), $\langle v_y'^2 \rangle$ (*b*), $\langle v_z'^2 \rangle$ (*c*), and $\langle v_x' v_y' \rangle$ (*d*) at different cross-stream positions. In all the cases the viscous relaxation time of the particle is less than the particle–particle collision time, $\tau_v < \tau_{c_{pp}}$, and $\phi = 9.44 \times 10^{-5}$. Simulation run 1, DNS (○); run 2, DNS (∗); run 4, DNS (◇); run 1, FFS (-·-); run 2, FFS (—); run 4, FFS (−−). Parameters for all the runs are given in table 1.

The velocity distribution functions for the case $\tau_v < \tau_{c_{pp}}$ are shown as a function of the particle fluctuating velocity in figure 3(*a*,*c*,*e*) for streamwise, wall-normal and spanwise components of particle velocity fluctuations. The distribution functions have been calculated in the central 10 % ($y^+ = 104.0$–115.5) of the channel, where the fluid root mean square velocities are nearly a constant. The first important results of this comparison is that the fluctuating force simulation is able to quantitatively capture the distribution of the particle velocities, and not just the moments of the velocity distribution. The second important result is that the fluctuating force simulation accurately captures the non-Gaussian nature of the velocity distribution in the wall-normal and spanwise directions that is observed in the direct numerical simulations. The agreement in all cases is quantitative up to about three decades of variation in the distribution function. To validate the efficiency of the fluctuating force model in capturing the particle velocity distribution function at different cross-stream positions, we have compared the distribution function of all three components of velocity fluctuation at three different cross-stream positions (A, B and C in figure 2) of the channel as shown in figure 16. We find that fluctuating force simulation predicts the distribution accurately for all the cases and shows the departure from Gaussian at all the locations. The particle velocity distributions in the wall-normal and spanwise directions (figure 16*b*,*c*) exhibit two distinct regimes: fast decay at low velocities due

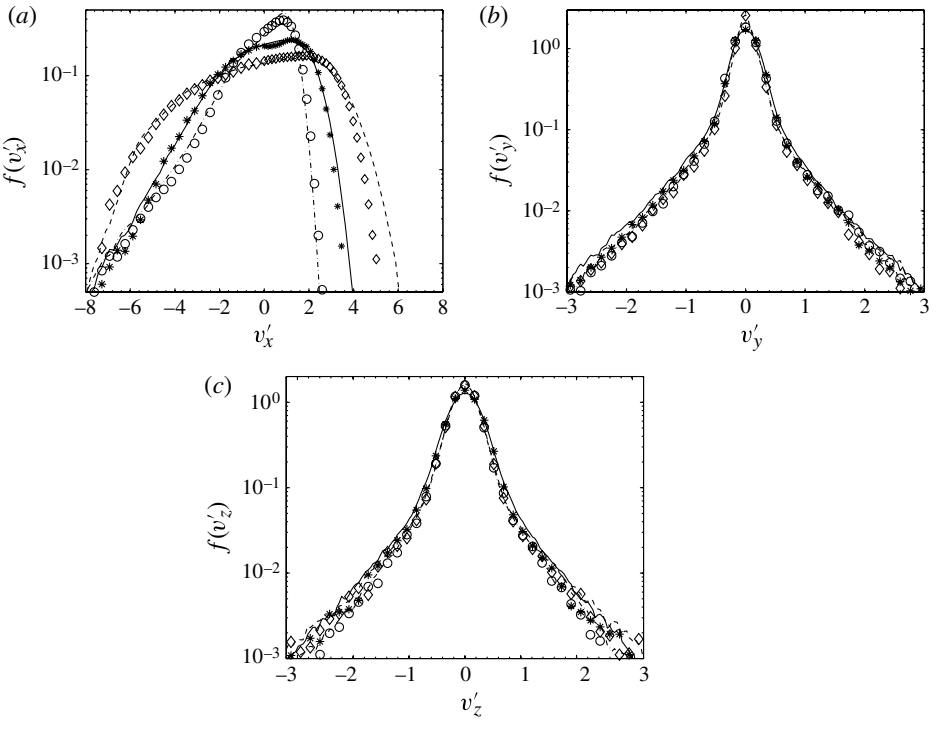

FIGURE 16. Particle velocity distribution function at different cross-stream positions of the channel for streamwise (a), wall-normal (b), and spanwise (c) components of velocity fluctuations. The viscous relaxation time of the particle is less than the particle–particle collision time, $\tau_v < \tau_{cpp}$, $\phi = 9.44 \times 10^{-5}$ and simulation run 2, $\tau_v = 355.3$, $\tau_{cpp} = 1650.3$ and $\tau_{c_{pw}} = 990.1$ at positions A, DNS ($\diamond$), FFS ($--$); B, DNS ($*$), FFS (—); C, DNS ($\circ$), FFS (-·-). Positions A, B and C are shown in figure 2. Parameters for run 2 are given in table 1.

to the effect of the fluid velocity fluctuations, and slow decay at larger velocities due to inter-particle collisions at all the cross-stream positions.

In the channel flow, the turbulent velocity fluctuations are highly anisotropic and inhomogeneous, and the fluctuation in the streamwise direction is much larger than that in the wall-normal and spanwise directions. We have analysed the source of particle velocity fluctuation at three different wall-normal positions (positions A, B and C in figure 2*b*). There could be three driving forces for the streamwise particle velocity fluctuations (Goswami & Kumaran 2010*b*). The first is due to the force exerted by the fluid turbulent velocity fluctuations in the streamwise direction, for which particle mean square velocity is expected to be scaled as $D_{xx}\tau_v$. The second mechanism is the transport of the particles across the streamline due to cross-stream (y) turbulent velocity fluctuations. The magnitude of the particle velocity fluctuation in the cross-stream direction is $(D_{yy}\tau_v)^{1/2}$, and this fluctuation transports the particle a distance $(D_{yy}\tau_v)^{1/2} \times \tau_v$ in the cross-stream direction. The streamwise mean square velocity difference due to that cross-stream transport is $(D_{yy}\tau_v)(\dot{\gamma}\tau_v)^2 \sim St_\gamma^2 (D_{yy}\tau_v)$, where $St_\gamma = \dot{\gamma}\tau_v$ is the Stokes number based on the mean strain rate. A third mechanism is due to particle collisions induced by the mean velocity gradient of the particle phase. The frequency of such collisions is proportional to $nd^2(\dot{\gamma}d)$, where $\dot{\gamma}$ is the mean velocity gradient for the particle phase, d is the particle diameter,

τ_v	St_γ	$\tau_v D_{xx}$	$\tau_v D_{yy}$	$(\tau_v D_{yy})St_\gamma^2$	$(\dot{\gamma}d)^2$	$\phi(\dot{\gamma}d)^2 St_\gamma^3$	T_{xx}
(*a*) At position A ($y^+ = 5.8$–17.3)							
177.66	44.31	2.00	0.026	51.57	0.234	1.927	8.05
355.32	54.50	1.00	0.013	39.00	0.089	1.355	6.36
532.98	63.70	0.67	0.009	35.52	0.054	1.314	5.33
710.64	68.13	0.50	0.007	30.48	0.035	1.035	4.25
(*b*) At position B ($y^+ = 34.7$–46.2)							
177.66	10.08	1.10	0.074	7.57	0.012	1.17×10^{-3}	4.38
355.32	15.30	0.55	0.037	8.73	0.007	2.37×10^{-3}	2.96
532.98	17.75	0.36	0.025	7.57	0.004	2.21×10^{-3}	2.32
710.64	23.66	0.27	0.019	10.43	0.002	2.96×10^{-3}	1.88
(*c*) At position C ($y^+ = 104.0$–115.5)							
177.66	1.056	0.196	0.040	0.045	1.33×10^{-4}	1.48×10^{-8}	1.83
355.32	1.331	0.098	0.020	0.035	5.29×10^{-5}	1.18×10^{-8}	1.74
532.98	1.535	0.065	0.013	0.031	3.13×10^{-5}	1.07×10^{-8}	1.57
710.64	1.597	0.049	0.010	0.025	1.90×10^{-5}	7.32×10^{-9}	1.41

TABLE 3. Expected magnitudes of the streamwise mean square velocity due to different sources of streamwise particle velocity fluctuations at positions A, B, C in the channel.

$\dot{\gamma}d$ is the velocity difference between particles on streamlines separated by one particle diameter, and n is the number density of the particles. When expressed in terms of the volume fraction $\phi \sim nd^3$, the collision frequency is $\phi\dot{\gamma}$. The transverse velocity fluctuation induced due to this collision is proportional to $\dot{\gamma}d$, and so the particle travels a distance $\dot{\gamma}d\tau_v$ in the horizontal direction due to the collision. The rate of increase in the fluctuating velocity due to collisions is $\phi\dot{\gamma}(\dot{\gamma}d)^2 St_\gamma^2$. The rate of decrease in the mean square of the streamwise fluctuations is $O(T_{xx}/\tau_v)$, where T_{xx} (the streamwise granular temperature) is the mean square of the streamwise particle velocity fluctuations. From this, we find that the granular temperature $T_{xx} \sim \phi(\dot{\gamma}d)^2 St_\gamma^3$, where the Stokes number $St_\gamma = \dot{\gamma}\tau_v$.

The expected velocity fluctuations due to these three mechanisms at locations A, B and C (figure 2*b*) are shown in table 3. It is clear that the dominant contributions are from the fluid turbulent velocity fluctuations in the cross-stream direction inducing streamwise particle velocity fluctuations at locations A and B, whereas the streamwise fluid turbulent velocity fluctuations provide the maximum contribution to T_{xx} at the centre of the channel, location C. The generation of particle velocity fluctuations due to collisions induced by mean shear, which scales as $(d\dot{\gamma})^2$, is not the largest source of fluctuations even at location A nearest to the wall of the channel, where the mean strain rate of the particles is the largest. At the centre of the channel, the value of T_{xx} is significantly larger than $\tau_v D_{xx}$ and $(\tau_v D_{yy})St_\gamma^2$, implying that the largest source of fluctuations is non-local (i.e. not only due to the sources of fluctuations at the centre of the channel) and the cross-stream motion of the particle plays an important role in magnifying the fluctuations at the centre. The opposite is true at location A, where T_{xx} is smaller than $(\tau_v D_{yy})St_\gamma^2$, due to the transport of T_{xx} from location A towards the centre of the channel.

We have verified that the second mechanism (streamwise fluctuations induced by particle transport and cross-stream velocity fluctuations of the particle phase)

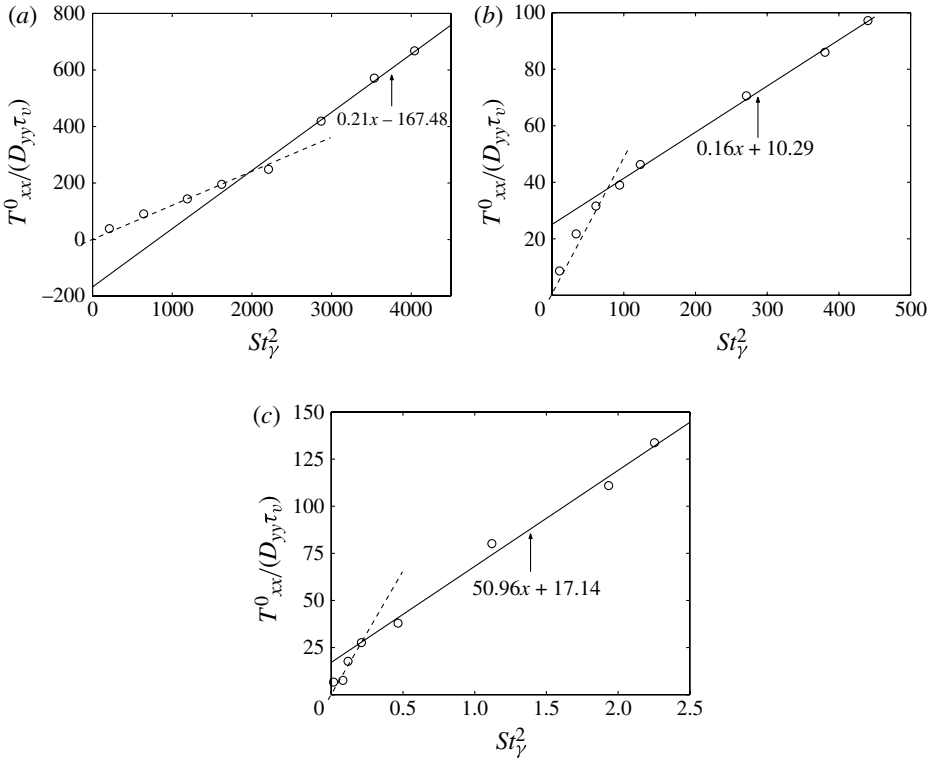

FIGURE 17. Particle velocity fluctuation in the streamwise direction in the presence of mean flow and cross-stream fluid velocity fluctuation but in the absence of streamwise fluid velocity fluctuation, when the viscous relaxation time of the particle is less than the particle–particle collision time, $\tau_v < \tau_{c_{pp}}$, $\phi = 9.44 \times 10^{-5}$ at position A (*a*), B (*b*) and C (*c*) in the channel (shown in figure 2).

is dominant by carrying out simulations where the streamwise turbulent velocity fluctuations are switched off, and only the cross-stream turbulent fluctuations are incorporated. The Stokes number in these simulations is changed by changing the particle density while keeping the flow velocity constant, which in turn changes the viscous relaxation time of the particles. The results for $T^0_{xx}/(D_{yy}\tau_v)$ versus St^2_γ, are shown in figure 17 at different wall-normal positions in the channel. The figures show two linear regimes. The linear fit at low Stokes number passes through the origin, as expected, because the streamwise velocity fluctuations should become zero when the strain rate is zero. The linear fit at high Stokes number, which is of primary interest in the present analysis, does have a non-zero intercept at zero Stokes number and also the slope of the fits varies from one wall-normal position of the channel to the other. The reason for such behaviour could be because fluctuations are not being generated locally, but are being transported across the channel from regions of high to low mean square velocities by a mechanism similar to conduction in fluids. We also consider the situation where streamwise particle velocity fluctuations are induced due to the streamwise diffusivity D_{xx} and also for the particle motion across streamlines due to the cross-stream turbulent fluctuations. In this case, our aim is to verify whether these two contributions are additive. Figure 18 shows that the contributions are not additive, since there is a maximum deviation of 40 % of the simulation results from

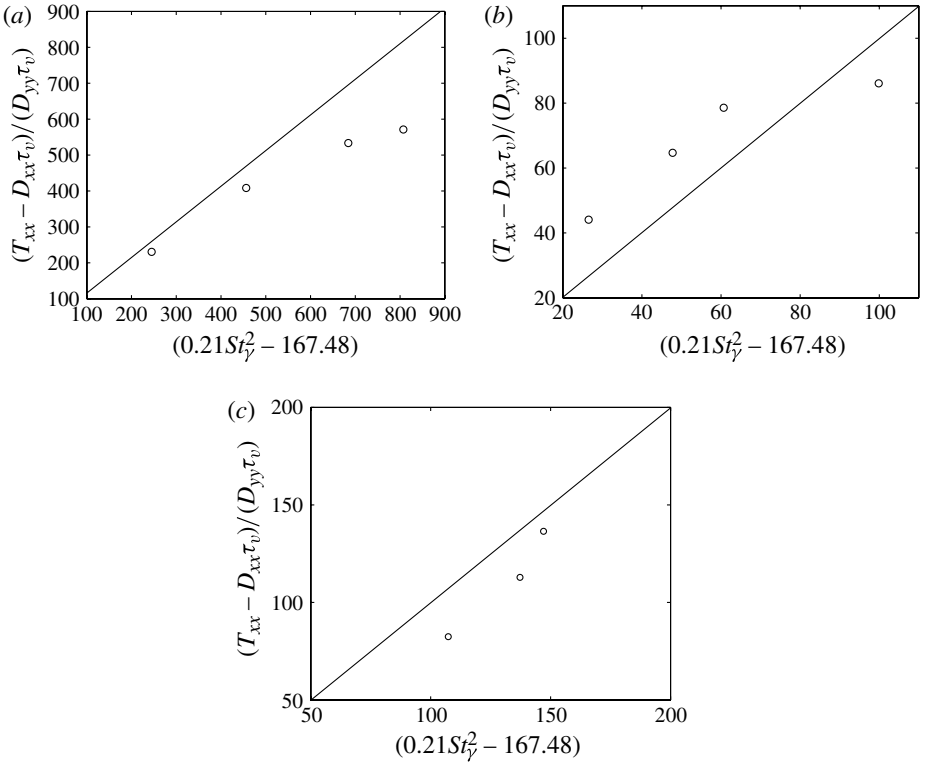

FIGURE 18. Scaling for streamwise velocity fluctuation in the presence of shear and the streamwise fluid velocity fluctuation to depict the contribution of the two sources at position A, B and C (shown in figure 2) in the channel. The viscous relaxation time of the particle is less than the particle–particle collision time, $\tau_v < \tau_{c_{pp}}$, $\phi = 9.44 \times 10^{-5}$.

the theoretical predictions. This is contrary to the situation for a shear-driven Couette flow (Goswami & Kumaran 2010*b*), where there is significantly less inhomogeneity in the cross-stream direction. This indicates that streamwise particle velocity fluctuations cannot simply be predicted by adding the contributions from those streamwise and cross-stream diffusivities.

Next, we analyse the cross-stream velocity fluctuations in the limit where the viscous relaxation time is small compared to the time between collisions. Cross-stream particle velocity fluctuations could be due to three reasons. One is cross-stream fluid velocity fluctuations. The second reason is the collisions between particles travelling on nearby streamlines with different mean velocities; this mechanism was analysed by Tsao & Koch (1995). The post-collisional cross-stream velocity is $O(d\dot{\gamma})$, and so one would expect the particle velocity fluctuations generated by this mechanism to be $O(d\dot{\gamma})$. The frequency of collisions due to this mechanism is $O((nd^2)(d\dot{\gamma}))$, where n is the number of particles per unit volume. Therefore, the rate of increase in the mean square of the fluctuating velocity due to collisions is $O((nd^2)(d\dot{\gamma})^3) \sim \phi\dot{\gamma}(d\dot{\gamma})^2$. The rate of decrease in the mean square of the cross-stream fluctuations is $O(T_{yy}/\tau_v)$, where T_{yy} (the cross-stream granular temperature) is the mean square of the cross-stream velocity fluctuations. From this, we find that the granular temperature $T_{yy} \sim \phi(d\dot{\gamma})^2 St_\gamma$, where the Stokes number $St_\gamma = (\dot{\gamma}\tau_v)$. The third mechanism for the generation of cross-stream fluctuations is the collisions induced by the streamwise

τ_v	St_γ	$\tau_v D_{yy}$	$(\dot{\gamma}d)^2$	$\phi(\dot{\gamma}d)^2 St_\gamma$	T_{xx}	$\phi(T_{xx}^{1/2}\tau_v/d)T_{xx}$	T_{yy}
(a) At position A ($y^+ = 5.8$–17.3)							
177.7	44.31	0.026	0.235	9.81×10^{-4}	8.05	0.197	0.159
355.3	54.50	0.013	0.089	4.57×10^{-4}	6.36	0.277	0.153
533.0	63.70	0.009	0.054	3.24×10^{-4}	5.33	0.319	0.152
710.6	54.82	0.007	0.022	1.16×10^{-4}	4.25	0.303	0.150
(b) At position B ($y^+ = 34.7$–46.2)							
177.7	10.08	0.074	0.012	1.15×10^{-5}	4.38	0.079	0.242
355.3	15.30	0.037	0.007	1.01×10^{-5}	2.96	0.088	0.195
533.0	17.75	0.025	0.004	7.00×10^{-6}	2.32	0.091	0.180
710.6	23.66	0.019	0.002	5.29×10^{-6}	1.88	0.089	0.163
(c) At position C ($y^+ = 104.0$–115.5)							
177.7	1.056	1.33×10^{-4}	6.25×10^{-5}	1.33×10^{-8}	1.83	0.021	0.175
355.3	1.331	5.29×10^{-5}	1.73×10^{-4}	6.64×10^{-9}	1.74	0.020	0.160
533.0	1.535	3.13×10^{-5}	3.13×10^{-5}	4.53×10^{-9}	1.57	0.017	0.156
710.6	1.597	1.90×10^{-5}	1.36×10^{-5}	2.87×10^{-9}	1.41	0.014	0.145

TABLE 4. Expected magnitudes of the cross-stream mean square velocity due to different sources of wall-normal particle velocity fluctuations at positions A, B and C in the channel.

velocity fluctuations. If T_{xx} is the mean square of the streamwise velocity fluctuations (granular temperature in the streamwise direction), then the frequency of collisions due to this mechanism is $(nd^2T_{xx}^{1/2})$. The post-collisional cross-stream velocity due to this mechanism is $O(\sqrt{T_{xx}})$, and so the rate of increase of the cross-stream fluctuations due to this mechanism is $O(nd^2T_{xx}^{3/2})$. The rate of decrease of the cross-stream velocity fluctuations due to viscous drag is $O(T_{yy}/\tau_v)$. A balance between these indicates that $T_{yy} \sim (nd^2T_{xx}^{1/2}\tau_v)T_{xx} \sim \phi\,(\sqrt{T_{xx}}\tau_v/d)T_{xx}$. The magnitude of particle velocity fluctuations due to these three mechanisms, as well as the mean square velocities, are shown in table 4's different wall-normal positions of the channel. From these, it is clear that the inter-particle collisions due to the streamwise velocity fluctuations provide the dominant contribution to the cross-stream velocity fluctuations, though the contribution due to the cross-stream turbulent diffusivity is also significant at location B and C. As in the case of streamwise fluctuations, we find that T_{yy} is smaller than $\phi\,(T_{xx}^{1/2}\tau_v/d)^{1/2}T_{xx}$ at location A, but the opposite is true at location C. This indicates that there is significant cross-stream transport from regions of high to low fluctuating velocities for the cross-stream fluctuations as well.

Next, we consider the case where the inter-particle collision time is less than the viscous relaxation time at a solid volume fraction of 7×10^{-4}. Figure 12(b) and figure 13 show the mean particle velocity and the mean slip velocity (scaled with Stokes terminal velocity) at different wall-normal positions in the channel, and figure 14 shows the concentration profile. It is found that the variation in the concentration and mean velocity is smaller when the collision time is small compared to the viscous relaxation time. This is because the fluctuations generated by inter-particle collisions transport mass and momentum across the flow, thus homogenizing the concentration and mean velocity fields. We also find that there is substantial slip at the wall of the channel, and the mean particle velocity is not zero at the wall. There is, once again, quantitative agreement between the complete DNS

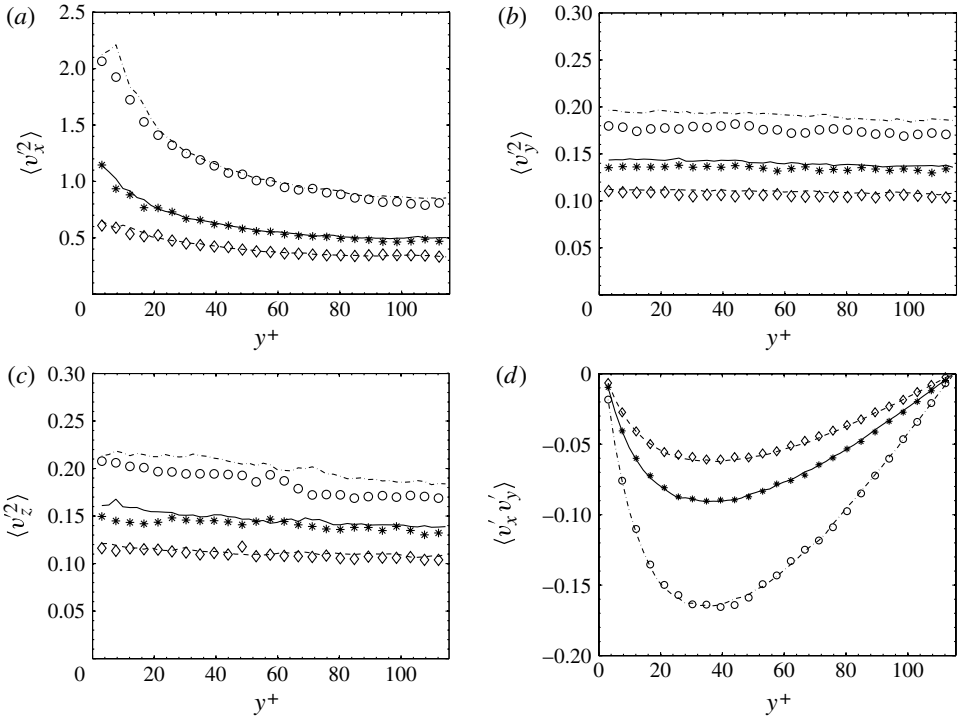

FIGURE 19. Variation of the second moments of the particle velocity distribution (*a*) $\langle v_x'^2 \rangle$, (*b*) $\langle v_y'^2 \rangle$, (*c*) $\langle v_z'^2 \rangle$, and (*d*) $\langle v_x' v_y' \rangle$ at different cross-stream positions. In all the cases the particle–particle collision time is less than the viscous relaxation time of the particle, $\tau_{c_{pp}} < \tau_v$, and $\phi = 7.0 \times 10^{-4}$. Simulation run 5, DNS (○); run 7, DNS (∗); run 8, DNS (◇); run 5, FFS (-··-); run 7, FFS (—); run 8, FFS (− −). Parameters for all the runs are given in table 1.

and the fluctuating force simulation. The ratio of the viscous relaxation time and the integral time scale varies in the range 10 to 30 for this regime. This explains the excellent agreement between the DNS and the Brownian dynamics simulations for wide range in Stokes number. Therefore, the assumption of Gaussian white noise for the fluctuating force is a good one in this case.

Figure 19 shows the variation of the mean square of the particle velocities in the three directions, and also the second moment of the fluctuating velocity $\langle v_x' v_y' \rangle$ for $\tau_{c_{pp}} < \tau_v$. In this case, collisions tend to equalize the root mean square velocities across the channel, therefore the variations across the channel are much less than those for $\tau_v < \tau_{c_{pp}}$. The mean square velocity in the streamwise direction is larger than that in the wall-normal and spanwise directions by a factor of ~ 5 in the centre of the channel, though the streamwise mean square velocity is much larger near the wall. This is due to an increase in the mean square of the fluid velocity fluctuations near the wall, which results in a greater fluctuating force in this region. An interesting observation is that $\langle v_y'^2 \rangle$, $\langle v_z'^2 \rangle$ and the concentration are nearly uniform across the channel. This implies that the component τ_{yy}^p of the streaming stress tensor for the particle phase, is nearly constant across the channel. (Note that at the very low volume fractions under consideration, the collisional stress is negligible in comparison to the streaming stress.) This implies that the net force exerted by the fluid on the particles in the y and z directions is negligible, because the gradient of the stress is equal to the net force. The component τ_{xy}^p is found to be non-zero, indicating that there is a local

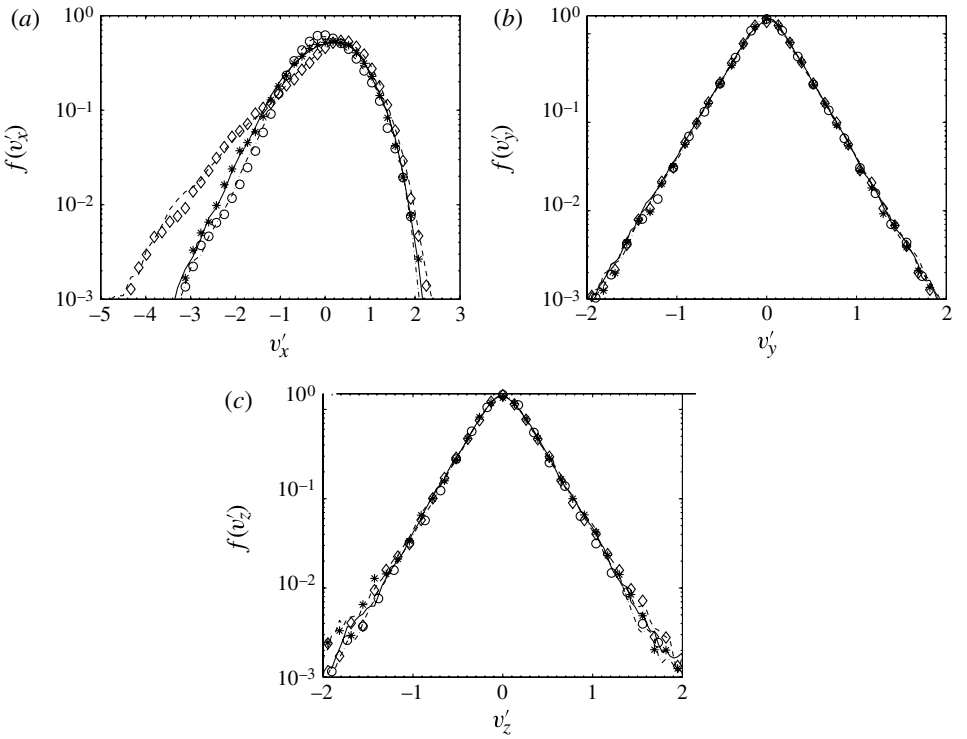

FIGURE 20. Particle velocity distribution function at different cross-stream positions of the channel for streamwise (*a*), wall-normal (*b*) and spanwise (*c*) components of velocity fluctuations. Particle–particle collision time is less than the viscous relaxation time of the particle, $\tau_{c_{PP}} < \tau_v$, $\phi = 7.0 \times 10^{-4}$, and simulation run 7, at positions A, DNS (◇), FFS (−−); B, DNS (∗), FFS (—); C, DNS (○), FFS (-·-). Positions A, B and C are shown in figure 2. Parameters for run 7 are given in table 1.

non-zero net force exerted by the fluid on the particles in the x direction. Therefore, the particle velocity fluctuations are driven by the force exerted by the fluid velocity fluctuations in the x direction, and the difference between the particle and fluid mean velocities; this is then transmitted to the cross-stream directions due to collisions. The results of the fluctuating force simulations are, once again, in quantitative agreement with those of the complete direct numerical simulations.

Figure 5(*a*,*c*,*e*) shows the distribution functions for the three directions. As found in the case of DNS, the particle velocity distribution function in all cases are non-Gaussian. The velocity distribution in the streamwise direction from DNS is asymmetric, and the asymmetric nature of the distribution is captured by the fluctuating force simulation. The distributions in the other two directions seem to show an exponential variation with velocity in the limit of high velocity; the fluctuating force simulation captures quantitatively the probability distribution function for the velocities even when the value of the distribution function is as small as 10^{-2}. The distribution function of all three components of velocity at three different cross-stream positions of the channel are compared in figure 20. This figure shows that the fluctuating force model quantitatively captures the distribution function along different cross-stream positions as well.

5. Conclusions

The objective of the present analysis was to model the dynamics of the particle phase in a channel flow of a turbulent gas–solid suspension using the fluctuating force model. In this model, the effect of fluid velocity fluctuations are replaced by a fluctuating force, whose distribution is given by Gaussian white noise. An implicit assumption in this model is that the viscous relaxation time of the particles is large compared to the correlation time of the fluid velocity fluctuations, so that the effect of the fluid on the particles can be represented as Gaussian white noise, therefore the analysis is restricted to relatively massive particles with high Stokes number. The Reynolds number based on the particle diameter and fluid density is relatively small (less than $\sim$10), so that the drag force can be described by a modification of Stokes' drag law. The strategy in the modelling procedure is to obtain the variance of this noise from the variance of the fluid velocity fluctuations in the gas phase evaluated using DNS. This fluctuating force is then incorporated into a Langevin simulation model for the particle phase alone, and the particle concentration, mean velocity and velocity variances are calculated. The results are compared with complete direct numerical simulations which incorporate the particles as well, in order to examine whether this model can be used for quantitative prediction of the dynamics of the particle phase in a gas–solid suspension.

A limitation of our calculation is that in the direct numerical simulations, we have only considered the effect of the fluid velocity fluctuations on the particle phase (one-way coupling), and we have neglected the effect of the particles on the fluid phase. This is because our objective is to model the effect of the turbulent velocity fluctuations on the dynamics of the particle phase, which can then be incorporated into theories for granular flows. This has enabled us to evaluate the fluid velocity fluctuations in a simulation where the particles do not exert any reverse force on the fluid phase. However, in a more comprehensive model, it is also necessary to examine the effect of particles on the fluid velocity fluctuations, since the modification of the fluid velocity fluctuations could, in turn, alter the fluctuating force on the particles. Therefore, this should only be considered as a first step in a more complete model where the effect of the particles on the fluid phase is also incorporated.

In Goswami & Kumaran (2010*b*), we modelled the Couette flow of a turbulent gas–particle suspension in the absence of gravity using the fluctuating force model, where the effect of the turbulent velocity fluctuations on the particle phase was replaced by white noise. This model gave quantitatively accurate results when the relaxation time of the particles is large compared to the fluid integral time scale. However, the Couette flow has some features which make it amenable to description by a simple model. Among these are the small mean velocity and the nearly constant root mean square of the fluctuating velocities at the centre of the channel; in addition, it was found that the acceleration distributions are also well described by Gaussian distributions in Couette flow. The objective of the present analysis was to examine whether a more complicated and realistic turbulent gas–particle flow, which is the pressure-driven flow in a channel, can be modelled using the fluctuating force model.

The flow in a channel is more complicated than Couette flow for a number of reasons. There is a sharp gradient in the mean fluid velocity near the wall of the channel, and the velocity increases to a maximum near the centre. The distribution of fluctuating velocities is highly anisotropic, and the root mean square velocity in the flow direction is much larger than that in the gradient and spanwise directions. In addition, there is substantial slip between the fluid and particle phase at the wall. A more important complication is that the root mean square velocity shows

large variations across the channel; it has a pronounced maximum near the wall, and decreases towards the centre of the channel. This is in contrast to Couette flow, where the root mean square velocity is approximately constant in the central region, and decreases to zero only within a thickness of ~ 5 wall units from the wall. Our simulations also show that the fluid velocity fluctuations are also anisotropic near the centre of the channel, and both the skewness and flatness are $O(1)$. The purpose of the present analysis was to examine whether a fluctuating force model can be used in a channel flow as well, since this would provide a first step towards wider application for industrially relevant systems such as fluidized and circulating beds.

For analysing the fluid velocity fluctuations, three regions in the channel of thickness ~ 10 wall units at different locations in the wall-normal direction were chosen, one of which was near the wall where the root mean square fluid velocity fluctuations pass through a maximum, the second was at the centre of the channel, and the third was in-between.

First, we considered the regime where the viscous relaxation time is smaller than the time between collisions. In the flow direction, the particle velocity and acceleration distributions were found to be highly skewed at the centre of the channel, but the skewness is less at the other two locations. The acceleration distributions in the other two directions were found to be close to Gaussian distributions at all locations, though the velocity distributions showed the slowly decaying tails (similar to those observed in Couette flow) due to collisions between particles induced by fluid velocity fluctuations in the flow direction. In the regime where the collision time is small compared to the viscous relaxation time, we find that the velocity distributions are different from Gaussian distributions, but the anisotropy in the distributions is less. It is also found that an estimate of the fluctuating particle acceleration distribution, obtained from the fluctuating velocity in the fluid, is in very good agreement with the actual acceleration distribution on the particles evaluated using DNS. A similar feature was observed in the case of Couette flow as well. However, it is necessary to examine whether this approximation is also valid when the effect of the particles on the fluid turbulence (reverse coupling) is included; the reverse coupling has not been included in the present calculation.

The time correlations of the fluid velocity fluctuations and the acceleration fluctuations on the particles were evaluated and compared. It was found that the time correlation functions for the fluid in the fixed Eulerian were not in agreement with the time correlation of the acceleration of the particles. However, the time correlations of the particle acceleration were in good agreement with the velocity time correlations in the fluid in a 'moving Eulerian' reference frame, moving with the mean velocity of the fluid. There are two reasons for this. Firstly, the particle mean velocity is close to the fluid mean velocity in most of the channel, though there is slip at the wall. The second reason is that the mean square of the spanwise and wall-normal components of particle fluctuating velocity is much smaller than the fluid fluctuating velocity. Due to this, it is sufficient to calculate the velocity time correlation in a reference frame moving with the fluid mean velocity. It should be noted that there is substantial slip between the particle mean velocity and the fluid mean velocity very close to the wall of the channel, between 1 and 10 wall units away from the wall. However, the mean square of the fluctuating velocity decreases to zero at the wall, and it is numerically small in the region 1–10 wall units away from the wall. Therefore, any errors due to the use of the moving Eulerian reference frame does not seem to affect the particle acceleration statistics in the fluctuating force simulations.

The variances of the fluctuating force were calculated from the fluid velocity fluctuations in a moving Eulerian reference frame, and these were inserted into the fluctuating force simulations. The results of the simulations were compared with the results of the DNS. In the limit where the viscous relaxation time is small compared to the time between collisions, it was found that the results of the two simulations for the mean velocity and the root mean square velocity in the flow direction are in very good agreement. When the viscous relaxation time is only about three times the fluid velocity autocorrelation time, there is a difference of $\sim 18\,\%$ in the results for the concentration field and the mean square velocities in the wall-normal and spanwise directions. When the particle viscous relaxation time is larger, there is quantitative agreement for the concentration, mean velocity and the mean square velocities.

In addition to the mean and the mean square velocities, we have also examined the velocity distribution functions at the centre of the channel. We find that the fluctuating force simulation is able to quantitatively capture the non-Gaussian nature of the velocity distribution at the centre of the channel. It should be noted that we have used a Gaussian force distribution in the fluctuating force simulation, whereas the actual distribution of the particle acceleration was found to be highly non-Gaussian in the direct numerical simulations. The reason for this agreement is as follows. The mean square fluid velocity in the centre of the channel is actually much smaller than the maximum mean square velocity at about twenty wall units away from the wall. Consequently, the acceleration fluctuations on the particles at the centre is small compared to that near the wall, and the source of fluctuating energy is primarily located in the region $\sim$10–20 wall units away from the wall, where the fluid velocity fluctuations pass through a maximum. The particle fluctuating velocity at the centre is primarily determined by the transport of particles across the flow from the wall region due to fluctuations, and the damping effect due to fluid drag. Since the fluid velocity distribution near the wall (at the position of maximum mean square fluid velocity) is a Gaussian distribution, this is accurately modelled in the fluctuating force model. Therefore the model is also able to capture, quantitatively, the fluctuations near the centre, though the acceleration distribution in the centre is not Gaussian.

The main conclusions of the present analysis are as follows.

(*a*) The fluctuating force model does accurately capture the particle dynamics in a channel flow, where there are large variances in the turbulent fluid velocity fluctuations across the channel, when one-way coupling (the effect of fluid on the particles) is included, provided care is taken in determining the autocorrelations of the fluid velocity fluctuations which are used to specify the Gaussian force distributions.

(*b*) It is necessary to evaluate the autocorrelations of the fluid velocity fluctuations in a 'moving Eulerian' reference frame, moving with the fluid mean velocity, instead of a fixed reference frame.

(*c*) The fluctuating force model quantitatively predicts the mean square of the particle velocity fluctuations. In addition, the form of the particle velocity distribution is well predicted even in situations where this is very different from a Gaussian distribution.

(*d*) From direct numerical simulations, the fluid velocity distributions are well approximated by Gaussian distributions in regions where the amplitude of the fluctuations is at a maximum. However, the fluid velocity distributions are very different from Gaussian distributions near the wall. Despite this, the fluctuating force model is successful near the wall as well, probably because the dominant contribution to the particle velocity fluctuations is the mean fluid shear, and not the turbulent fluctuations (which decrease to zero as the wall is approached).

It is necessary to carry out further research to examine whether the model is applicable in the presence of two-way coupling, where the effect of the particles on the fluid is incorporated.

The authors would like to thank the Department of Science and Technology, Government of India, for financial support.

Appendix. Fluctuating force model

In a discrete particle simulation (event-driven simulations, for example), the collision term is explicitly modelled in the form of instantaneous collisions between particles. The effect of the mean shear is also explicitly included due to the variation of the particle mean velocity with position. Therefore, it is necessary to modify the rules for particle advancement between collisions in order to include the effect of the random noise (representing the diffusivity in (4.1)) and the particle drag (which is the fourth term on the left in (4.1)). If we consider a steady state in which the mean shear and collisions are neglected, then the Boltzmann equation (4.1) reduces to

$$\frac{\partial f(\boldsymbol{v})}{\partial t} = \frac{1}{\tau_v}\frac{\partial\,(v_i f(\boldsymbol{v}))}{\partial\, v_i} + D_{ij}(\boldsymbol{x})\frac{\partial^2 f(\boldsymbol{v})}{\partial\, v_i \partial\, v_j}. \tag{A 1}$$

Equation (A 1) is equivalent to the Fokker–Planck equation, with the position-dependent coefficient of diffusion in velocity space, $D_{ij}(\boldsymbol{x})$, given by

$$D_{ij}(\boldsymbol{x}) = \int_0^\infty \mathrm{d}t' \,\langle a_i'(t') a_j'(0)\rangle = \frac{1}{\tau_v^2}\int_0^\infty \mathrm{d}t' \,\langle u_i'(t') u_j'(0)\rangle\,. \tag{A 2}$$

Here $\boldsymbol{a}'$ is the acceleration fluctuation, which is equal to $\boldsymbol{u}'/\tau_v$ if we only consider the acceleration due to the fluid velocity fluctuations and assume Stokes' law. Implicit in (A 2) is the assumption that the decay time for the fluid velocity fluctuations is small compared to the viscous relaxation time or the collision time, so that the effect of fluid velocity fluctuations can be accurately represented by Gaussian white noise. The diffusion tensor D_{ij} is a symmetric tensor, and has dimensions of $(\mathrm{length}^2/\mathrm{time}^3)$. When the fluid is driven by the shear in the x–y plane, the components D_{xz} and D_{yz} are zero because the probability distribution for the velocity fluctuation in the z direction is an even function of u_z'.

The detailed description of the Langevin formulation of particle equation of motion is given in Goswami & Kumaran (2010*b*). In the case of particle suspension in a gravity-driven channel flow, the equation for particle motion between collisions is modified as follows:

$$\frac{\mathrm{d}v_i}{\mathrm{d}t} = -\frac{v_i - \bar{u}_i(\boldsymbol{x}_p)}{\tau_v} + F_i(t) + g e_x, \tag{A 3}$$

where $\bar{u}_i(\boldsymbol{x}_p)$ is the mean velocity at the local particle position, F_i is a stochastic force which is generated due to turbulence fluctuations. The force magnitudes cannot be generated in the usual manner used for isotropic Gaussian noise, because the off-diagonal component D_{xy} of the diffusion matrix in (A 2) is non-zero. The magnitude of the force is determined by generating three independent normal random deviates, ζ_1, ζ_2 and ζ_3, with zero mean and unit variance. The components of the

force, F_i, are then expressed as

$$F_x = \frac{\sqrt{2D_{xx}}\zeta_1}{\sqrt{\Delta t}}, \tag{A 4}$$

$$F_y = \frac{\sqrt{2D_{yy}}}{\sqrt{\Delta t}}\left(\frac{D_{xy}\zeta_1}{\sqrt{D_{xx}D_{yy}}} + \zeta_2\sqrt{1-\frac{D_{xy}^2}{D_{xx}D_{yy}}}\right), \tag{A 5}$$

$$F_z = \frac{\sqrt{2D_{zz}}\zeta_3}{\sqrt{\Delta t}}. \tag{A 6}$$

Equation (A 3) is combined with instantaneous collisions when two particles come in contact using the collision laws for spherical elastic particles, to carry out the 'fluctuating force' simulation for the particle phase.

REFERENCES

ARMENIO, V. & FIOROTTO, V. 2001 Equation of motion for a small rigid sphere in a non-uniform flow. *Phys. Fluids* **13**, 2437.

BALACHANDAR, S. & EATON, J. K. 2010 Turbulent dispersed multiphase flow. *Annu. Rev. Fluid Mech.* **42**, 111–133.

BEC, J., BIFERALE, L., BOFFETTA, G., CELANI, A., CENCINI, M., LANOTTE, A., MUSACCHIO, S. & TOSCHI, F. 2006 Acceleration statistics of heavy particles in turbulence. *J. Fluid Mech.* **550**, 349–358.

BEC, J., BIFERALE, L., BOFFETTA, G., CENCINI, M., LANOTTE, A. S. & TOSCHI, F. 2010 Intermittency in the velocity distribution of heavy particles in turbulence. *J. Fluid Mech.* **646**, 527–536.

CANUTO, C., HUSSAINI, M. & ZANG, T. 1988 *Spectral Methods in Fluid Dynamics*. Springer.

CARLIER, J. P., KHALIJI, M. & OSTERLE, B. 2005 An improved model for anisotropic dispersion of small particles in turbulent shear flows. *Aerosol Sci. Technol.* **39**, 196–205.

DINAVAHI, S. P. G. 1992 Probability density functions in turbulent channel flow. Tech. Rep. 4454.

ELGHOBASHI, S. & TRUESDELL, G. C. 1992 Direct simulation of particle dispersion in a decaying isotropic turbulence. *J. Fluid Mech.* **242**, 655.

ELGHOBASHI, S. & TRUESDELL, G. C. 1993 On the two-way interaction between homogeneous turbulence and the dispersed solid particles. Part 1. Turbulence modification. *Phys. Fluids* A **5**, 1790.

FESSLER, J. R., KULICK, J. D. & EATON, J. K. 1994 Preferential concentration of heavy particles in a turbulent channel flow. *Phys. Fluids* **6**, 3742–3749.

FEVRIER, P., SIMONIN, O. & SQUIRES, K. D. 2005 Partitioning of the particle velocities in gas–solid turbulent flows into a continuous field and a spatially uncorrelated random distribution: theoretical formalism and numerical study. *J. Fluid Mech.* **533**, 1–46.

FOUXON, I. & HORVAI, P. 2008 Separation of heavy particles in turbulence. *Phys. Rev. Lett.* **100**, 040601.

GERASHCHENKO, S., SHARP, N. S., NEUSCAMMAN, S. & WARHAFT, Z. 2008 Lagrangian measurements of inertial particle accelerations in a turbulent boundary layer. *J. Fluid Mech.* **617**, 255–281.

GIBSON, J. F. 2007 *Channelflow: A Spectral Navier–Stokes Simulator in C++*. Georgia Institute of Technology.

GORE, R. A. & CROWE, C. T. 1989 Effect of particle size on modulating turbulent intensity. *Intl J. Multiphase Flow* **15**, 279.

GOSWAMI, P. S. & KUMARAN, V. 2010*a* Particle dynamics in a turbulent particle–gas suspension at high Stokes number. Part 1. Velocity and acceleration distributions. *J. Fluid Mech.* **646**, 59–90.

GOSWAMI, P. S. & KUMARAN, V. 2010*b* Particle dynamics in a turbulent particle–gas suspension at high Stokes number. Part 2. The fluctuating force model. *J. Fluid Mech.* **646**, 91–125.

GOSWAMI, P. S. & KUMARAN, V. 2011 Particle dynamics in the channel flow of a turbulent particle–gas suspension at high Stokes number. Part 2. Comparison of fluctuating force simulations and experiments. *J. Fluid Mech.* **687**, 41–71.

KHALITOV, D. A. & LONGMIRE, E. K. 2003 Effect of particle size on the velocity correlations in turbulent channel flow. *FEDSM200345730, 445, ASME/JSME Joint Fluid Engineering Conference* Honolulu, 2003.

KIM, J., MOIN, P. & MOSER, R. 1987 Turbulence statistics in fully developed channel flow at low Reynolds number. *J. Fluid Mech.* **177**, 133–166.

KLEISER, L. & SCHUMANN, U. 1980 Treatment of incompressibility and boundary conditions in 3D numerical spectral simulations of plane channel flows. In *Proceedings of the 3rd GAMM Conference on Numerical Methods in Fluid Mechanics,* vol. 2 (ed. E. H. Hirschel). pp. 165–173.

KRAICHNAN, R. H. 1958 Irreversible statistical mechanics of incompressible hydromagnetic turbulence. *Phys. Rev.* **109**, 1407–1422.

KULICK, J. D., FESSLER, J. R. & EATON, J. K. 1994 Particle response and turbulence modification in a fully developed channel flow. *J. Fluid Mech.* **277**, 109–134.

KUMARAN, V. 2003 Stability of a sheared particle suspension. *Phys. Fluids* **15**, 3625–3637.

LAVEZZO, V., SOLDATI, A., GERASHCHENKO, S., WARHAFT, Z. & COLLINS, L. R. 2010 On the role of gravity and shear on inertial particle accelerations in near-wall turbulence. *J. Fluid Mech.* **658**, 229–246.

LI, Y. & MCLAUGHLIN, J. B. 2001 Numerical simulation of particle-laden turbulent channel flow. *Phys. Fluids* **13**, 2957.

MAXEY, M. R. & RILEY, J. J. 1983 Equation of motion for a small rigid sphere in a non-uniform flow. *Phys. Fluids* **26**, 883.

RILEY, J. J. & PATTERSON, G. S. 1974 Diffusion experiments with numerically integrated isotropic turbulence. *Phys. Fluids* **17**, 292.

ROUSON, D. W. I. & EATON, J. K. 2001 On the preferential concentration of solid particles in turbulent channel flow. *J. Fluid Mech.* **428**, 149.

SQUIRES, K. D. & EATON, J. K. 1990 Particle response and turbulence modification in isotropic turbulence. *Phys. Fluids* A **2**, 1191.

SQUIRES, K. D. & EATON, J. K. 1991 Preferential concentration of particles by turbulence. *Phys. Fluids* A **3**, 1169.

TANAKA, T. & EATON, J. K. 2008 Classification of turbulence modification by dispersed spheres using a novel dimensionless number. *Phys. Rev. Lett.* **101**, 114502.

TSAO, H.-K. & KOCH, D. L. 1995 Shear flows of a dilute gas–solid suspension. *J. Fluid Mech.* **296**, 211–245.

YAMAMOTO, Y., POTTHOFF, M., TANAKA, T., KAJISHIMA, T. & TSUJI, Y. 2001 Large-eddy simulation of turbulent gas–particle flow in a vertical channel: effect of considering interparticle collisions. *J. Fluid Mech.* **442**, 303–334.